Cell Systems

A Blueprint for a Synthetic Genetic Feedback Controller to Reprogram Cell Fate

Graphical Abstract

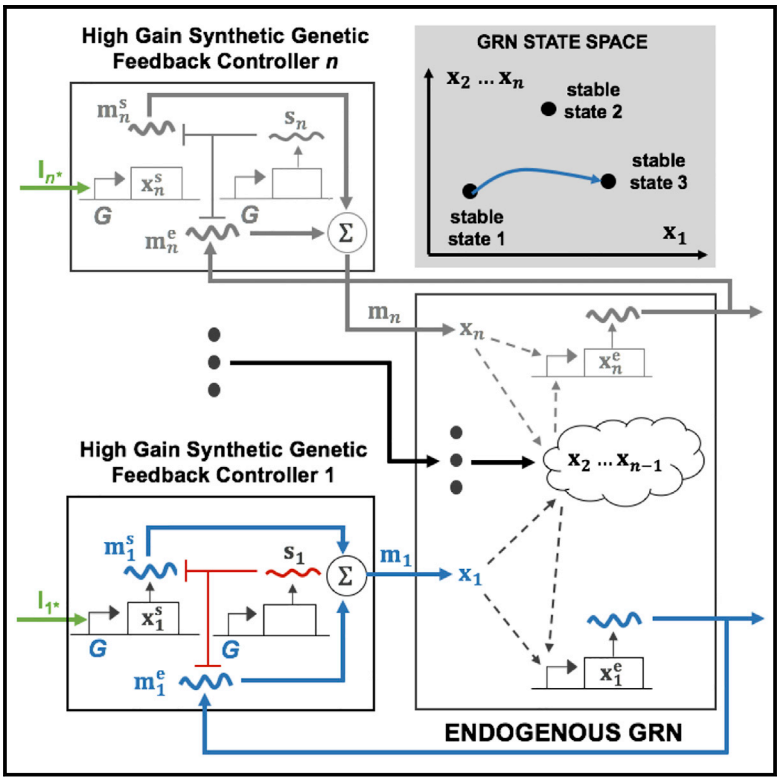

Highlights

- Control of TFs in a GRN is a critical aspect of directing cell fate
- Control via fixed overexpression relies on endogenous GRN dynamics
- High gain feedback overexpression control is robust to GRN dynamics
- Controller can be realized with a synthetic genetic circuit using siRNA technology

Authors

Domitilla Del Vecchio, Hussein Abdallah, Yili Qian, James J. Collins

Correspondence

ddv@mit.edu

In Brief

This work introduces a synthetic genetic feedback controller that enables accurate steering of cellular transcription factor concentrations to desired values. The controller's properties may have applications for directing or reprogramming cell fate.

Del Vecchio et al., 2017, Cell Systems *4*, 109–120
January 25, 2017
http://dx.doi.org/10.1016/j.cels.2016.12.001

Cell Systems
Math | Bio

A Blueprint for a Synthetic Genetic Feedback Controller to Reprogram Cell Fate

Domitilla Del Vecchio,[1,2,9,*] Hussein Abdallah,[3] Yili Qian,[1] and James J. Collins[2,4,5,6,7,8]
[1]Department of Mechanical Engineering, MIT, Cambridge, MA 02139, USA
[2]Synthetic Biology Center, MIT, Cambridge, MA 02139, USA
[3]Department of Electrical Engineering and Computer Science, MIT, Cambridge, MA 02139, USA
[4]Institute for Medical Engineering and Science, MIT, Cambridge, MA 02139, USA
[5]Department of Biological Engineering, MIT, Cambridge, MA 02139, USA
[6]Harvard-MIT Program in Health Sciences and Technology, Cambridge, MA 02139, USA
[7]Broad Institute of MIT and Harvard, 415 Main Street, Cambridge, MA 02142, USA
[8]Wyss Institute for Biologically Inspired Engineering, Harvard University, 3 Blackfan Circle, Boston, MA 02115, USA
[9]Lead Contact
*Correspondence: ddv@mit.edu
http://dx.doi.org/10.1016/j.cels.2016.12.001

SUMMARY

To artificially reprogram cell fate, experimentalists manipulate the gene regulatory networks (GRNs) that maintain a cell's phenotype. In practice, reprogramming is often performed by constant overexpression of specific transcription factors (TFs). This process can be unreliable and inefficient. Here, we address this problem by introducing a new approach to reprogramming based on mathematical analysis. We demonstrate that reprogramming GRNs using constant overexpression may not succeed in general. Instead, we propose an alternative reprogramming strategy: a synthetic genetic feedback controller that dynamically steers the concentration of a GRN's key TFs to any desired value. The controller works by adjusting TF expression based on the discrepancy between desired and actual TF concentrations. Theory predicts that this reprogramming strategy is guaranteed to succeed, and its performance is independent of the GRN's structure and parameters, provided that feedback gain is sufficiently high. As a case study, we apply the controller to a model of induced pluripotency in stem cells.

INTRODUCTION

In multistable gene regulatory networks, an individual network's state at any moment in time, as determined by the concentrations of the network's transcription factors (TFs), can be found, by definition, in multiple stable steady states. According to Waddington's view of cell differentiation (Waddington, 1957), each of the stable steady states of a gene regulatory network involved with development can be associated with a different cell phenotype and transitions between different phenotypes, as induced by external stimuli or noise, represent cell fate decisions (Wang et al., 2011). Our ability to direct or reprogram cell fate usually relies on artificially triggering specific state transitions with appropriate, known artificial perturbations and stimuli (Huang, 2009).

Overexpression of a known cocktail of TFs is a common and experimentally practical perturbation that successfully induces cell fate reprogramming in a number of instances (Graf and Enver, 2009). In these experiments, TF concentration is "preset," that is, it is increased over endogenous levels by experimental manipulations done before the experiment began and cannot be iteratively adjusted. The success rate of methods that rely on preset overexpression of transcription factors remains very low across a range of prefixed overexpression reprogramming methods (Morris and Daley, 2013; Schlaeger et al., 2015; Goh et al., 2013; Xu et al., 2015). We suggest that this is due to the fact that successful transitions between states using preset overexpression of TFs depend on the natural network's dynamics. Because there is no general guarantee that a given network's dynamics will allow transitions to the desired target state under the imposed perturbations, preset overexpression may not result in the desired outcome. For example, when the network motif is cooperative (that is, all existing mutual regulatory interactions are positive) and the target state is not maximal, achieving it will be difficult using preset overexpression (this is demonstrated mathematically below). A method for artificially enabling transitions between stable states that does not depend on the natural network's dynamics would overcome the network's natural limitations and allow for more efficient reprogramming.

In this paper, we address this problem by designing a general-purpose synthetic genetic feedback controller that can steer the concentrations of the network's TFs to any desired target values. This is done independently of the gene regulatory network's structure and parameters, provided the feedback gain is sufficiently high. With our approach, the overexpression level of TFs is not preset; instead, it is adjusted by the genetic feedback controller based on the discrepancy between the TF's current concentration and its desired concentration in the target state.

Our design has two components that we will discuss in detail and is depicted graphically in Figure S3A: a synthetic genetic controller circuit that globally stabilizes the concentration of

TFs to a value encoded by inducers' levels (inner loop control) and an in silico adjustment of the inducers' levels performed at steady state to decrease the discrepancy with the target TFs' concentrations (outer loop control). In particular, the controller implements feedback overexpression of each TF by concurrently realizing a large (inducible) production rate and a large degradation rate. The net result of these two large opposing forces is that the concentration of the TF approaches a well-defined "proportion" between the (synthetically realized) production and degradation rates, independently of the network that also regulates the TF. Because this proportion can be adjusted by an inducer, the inducer level uniquely dictates the TF's target concentration. The outer loop control measures the concentration of the TF after it has reached the steady state imposed by the current inducer level and compares it to the target concentration to determine the appropriate inducer level's adjustment. We demonstrate the performance of this general-purpose genetic feedback controller through mathematical analysis and simulations. As predicted from theory, simulation results show that we can trigger state transitions in multistable gene regulatory networks in which preset overexpression fails.

As a case study, in the Biology Box, we discuss the potential application of the controller to the problem of induced pluripotent stem cell (iPSC) reprogramming (Graf and Enver, 2009; Takahashi and Yamanaka, 2016). In particular, we illustrate simulation results in which the controller is employed to trigger transitions to the intermediate pluripotent state in a two-node network motif found in the core pluripotency gene regulatory network. Because this network includes positive regulatory interactions, steering TF concentrations to intermediate levels may not be possible with preset overexpression if these interactions dominate the network's behavior. In this case, the controller may guarantee higher success rates during iPSC reprogramming. More broadly, we discuss how the controller, owing to its unique ability to accurately steer and hold the concentrations of TFs at inducer-encoded levels, may be employed as a discovery tool for iPSC reprogramming.

RESULTS

Reprogramming of Cooperative Gene Networks through Preset Overexpression

In this section, we motivate the need for methods that can trigger desired state transitions in multistable gene regulatory networks independently of their natural dynamics. We mathematically describe the problem of triggering state transitions through preset overexpression of the gene regulatory network's TFs and demonstrate that this approach is not guaranteed to be successful. We use the specific example of cooperative network motifs, wherein TFs positively regulate each other. These motifs are of particular interest because they play a central role in the gene regulatory networks that control pluripotency (Boyer et al., 2005; Jaenisch and Young, 2008; Kim et al., 2008).

We consider ordinary differential equation (ODE) models of gene regulatory networks with n TFs, $x_1 \ldots, x_n$ in which overexpression of TF x_i is modeled as an external "input" u_i directly increasing the rate of production of the TF. Letting x_i denote the concentration of TF x_i and letting $x = (x_1, \ldots, x_n)$ represent the state of the network, we write:

$$\Sigma_u: \quad \frac{dx_i}{dt} = f_i(x, u_i), \quad \text{with } f_i(x, u_i) = H_i(x) - \gamma_i x_i + u_i, \quad i \in \{1, \ldots, n\}, \qquad \text{(Equation 1)}$$

in which $H_i(x)$ is the Hill function that captures the regulation of x_i by the networks' TFs (Del Vecchio and Murray, 2014), γ_i is the constant decay rate due to dilution (cell growth) and/or degradation, and $u_i \geq 0$. In the sequel, we let $u = (u_1, \ldots, u_n)$. When $u = 0$, the system in Equation 1, referred to as Σ_0, describes the natural network's dynamics without external intervention. We have neglected the mRNA dynamics to simplify notation, assuming that mRNA quickly reaches its quasi-steady state (Alon, 2007). This assumption can be made without loss of generality, as the analysis and results that follow hold independently of it. Within this model, the process of reprogramming the network's state to a target stable state S_0 can be qualitatively described as in Figure 1A. For illustration purposes, let us assume that the model with no input, Σ_0, has three stable steady states S_0, S_1, and S_2, although, in general, it can have many more. Because these are stable, they each have a region of attraction such that if the system's state x is initialized in the region of attraction of S_1 (S_0 or S_2, respectively), then the system's trajectory $x(t)$ will eventually approach S_1 (S_0 or S_2, respectively). When a constant overexpression rate u is applied, the landscape of steady states changes. For reprogramming the network to S_0, one would like the perturbed system Σ_u to have a unique globally stable steady state S_0' that lies in the region of attraction of S_0 (center plot of Figure 1A). In this case, sufficiently prolonged perturbation will lead the trajectory of the system starting from any initial state $x(0)$ to approach S_0'. Because S_0' lies in the region of attraction of S_0, the trajectory will ultimately converge to S_0 when perturbation is removed, thereby successfully reprogramming Σ_0 to S_0 (right plot of Figure 1A). In such cases where the perturbed system has a unique stable steady state in the region of attraction of the target state S_0, we will say that the system is strongly reprogrammable to S_0.

In the case of a cooperative network, the signs of the mutual regulatory interactions, if present, are positive, while autoregulatory loops can have any sign (Figure 1B). Referring to Equation 1, for a cooperative network we have the following properties:

(1) $\partial f_i / \partial u_i \geq 0$ (positive perturbation): increasing the input increases the production rate of the TFs;
(2) $\partial H_i(x) / \partial x_i \geq 0$ for $i \neq j$ (positive regulation): either TF i is not regulated by TF j or it is positively regulated by it. This also implies that $\partial f_i / \partial x_j \geq 0$, for all $i \neq j$, leading to a cooperative monotone system (Smith, 1995; Angeli and Sontag, 2003).

The set of stable steady states in a monotone cooperative system always has a maximal element, which is a stable steady state whose components are all greater than the corresponding components of all other stable steady states. Referring to Equation 1, the state is the tuple $(x_1, \ldots, x_n)$ whose i-th component x_i is the concentration of TF x_i. A stable steady state is maximal if each concentration x_i in that state is greater than the concentration x_i found in another stable steady state. For example, if we

Biology Box. Application to Induced Pluripotent Stem Cell Reprogramming

The core gene regulatory network responsible for the maintenance of pluripotency in iPSCs is composed of three TFs, Oct4, Sox2, and Nanog (pluripotency TFs), that mutually activate each other while also self-activating (Boyer et al., 2005; Jaenisch and Young, 2008; Kim et al., 2008) (Figure B1A). This core network is embedded in a larger network that includes competitive repressions between the pluripotency TFs, lineage specifiers, or growth TFs (Thomson et al., 2011; Niaken et al., 2010; Chambers et al., 2003; Niwa et al., 2005; Herberg et al., 2014). Reprogramming somatic cells to pluripotency has been performed by overexpressing pluripotency TFs (Takahashi and Yamanaka, 2006) and by adding chemical stimuli in order to force higher TF concentrations found in the pluripotent state (Theunissen and Jaenisch, 2014).

It has been proposed that an imbalance of lineage specifying TFs leads to undesirable fates, which suggests that accurate control of these lineage specifiers is key to higher reprogramming success rates (Shu et al., 2013). Among the pluripotency TFs, Oct4 plays a primary role in determining transitions in and out of pluripotency (Radzisheuskaya et al., 2013). Oct4 is abundant in the inner cell mass, downregulated in the trophectoderm, and upregulated in the primitive endoderm (Niwa et al., 2000; Palmieri et al., 1994). Stoichiometric balancing of overexpressed TFs substantially influences quality of iPSCs and the success rate of the process (Carey et al., 2011), which is fairly low and shows very high latency (Hanna et al., 2009, 2010). These observations suggest a landscape of cell fates in which the pluripotent state is associated with intermediate concentrations of Oct4, as shown in Figure B1B.

These studies indicate that accurate and timely stabilization of the concentrations of pluripotency TFs and lineage specifiers to within desired ranges may improve the rate and decrease the latency of iPSC reprogramming. In particular, if the pluripotency network is dominated by positive regulatory interactions and pluripotency is associated with intermediate Oct4 concentrations, then low success rates may be a symptom of not being able to stably reach target Oct4 concentrations with standard open loop overexpression strategies. As such, the controller we describe may guarantee a higher reprogramming success rate.

To illustrate this point, we consider the problem of reprogramming a simplified lumped, two-node model of the pluripotency network (Figure B1A). This model focuses on Oct4 for the reasons mentioned above and on Nanog because its high concentration is characteristic of pluripotency (Hanna et al., 2009). The model includes mutual positive regulation of Oct4 and Nanog (Boyer et al., 2005) and the effective repression from Oct4 to Nanog that results from Oct4 activating Gata6 (mesendodermal lineage specifier) and Gata6 repressing Nanog (Shu et al., 2013). For analysis, we consider a representative instance of this system with three stable steady states: one associated with the trophectoderm (TR), with low concentrations of Nanog and Oct4, one associated with the primitive endoderm (PE), with low Nanog and high Oct4 concentrations, and one associated with pluripotency (PL), with high Nanog and intermediate Oct4 concentrations (Figure B1B). In this model, the positive interaction from Oct4 to Nanog dominates at lower concentrations of Oct4 (around the TR and PL states) while the negative interaction dominates at higher Oct4 concentrations (around the PE state). Therefore, we expect from theory that reprogramming the system from TR to PL will require a specific intermediate range of overexpression. Because the objective of this illustration is to assess the performance of the controller in a case where preset overexpression fails, we consider a parametrization of the two-node gene regulatory network in which no preset overexpression level exists to reprogram the system from TR to PL (Figure B1C).

Stochastic simulations, in which feedback overexpression is implemented through the controller in Figure 3D for both TFs, show that the network state can be steered from TR to PL and be held there despite stochastic fluctuations while the controller is on (Figure B1D). We have captured biochemical reaction noise by using the chemical Langevin equation (CLE) model (Gillespie, 2000) (see "Stochastic Model" in the STAR Methods). The variance of the trajectories while the controller is acting is smaller than that resulting after the controller is shut down, which is determined by the natural gene regulatory network's dynamics (Figure B1D). This is expected from theory as mathematically demonstrated for a simple model of the controller (see "High Gain and Noise in the Genetic Controller" in the STAR Methods).

If each stochastic realization is viewed as a single cell's trajectory, these results suggest that the controller may decrease cell-to-cell variability, although a number of issues regarding stochastic properties require further study. First, the simulations are based on CLEs and therefore do not capture phenomena that become more prominent at lower molecular counts, such as stochastically induced multimodality, nor the observed high variability in reprogramming latency, which is the subject of intense investigation (Hanna et al., 2009). In addition, the model used here does not include chromatin dynamics, which may substantially contribute to stochasticity and latency observed in reprogramming experiments (Soufi et al., 2012) and challenge the standard adiabatic TF/promoter binding assumption on which gene regulation models are based (Feng and Wang, 2012). Moreover, differences in parameter values across cells should be incorporated in stochastic models. Finally, the target state S_0 in practice corresponds to a distribution of target TF concentrations rather than to a unique concentration (Cahan and Daley, 2013).

In the simulations of Figure B1, the inducer concentrations in the controller were set to make the target state x^* close to PL (Equation 6). From a practical standpoint, experimentalists could screen for inducer concentrations that, with the controller in place, deliver higher reprogramming success rates and then use these in reprogramming experiments. This is a simpler alternative to the outer loop feedback adjustment of the inducer's concentration shown in Figure S3A and discussed in "Outer Loop Feedback Control for Adjusting x_i^*" in the STAR Methods.

Figure S3B shows that the outer loop controller steers TF concentrations through various steady-state level. If the phenotype of the cell is dictated by the concentration of the TFs under control (Oct4 and Nanog, in this example), then all trajectories ending with the pluripotent concentrations of these TFs will lead to pluripotency. If, instead, additional uncontrolled pluripotency TFs or lineage specifiers in the pluripotency gene regulatory network are necessary to dictate the pluripotent phenotype, then these may lead the gene regulatory network to different states depending on the path followed by the controlled TFs' concentrations. These states, in turn, may prime cells to non-pluripotent lineages despite the controller completing its task and steering the reprogramming TFs under its control to the pluripotent concentrations.

While this is a limitation, it is also a feature that may be used as a discovery tool for both uncovering minimal sets of TFs that dictate pluripotency and for revealing whether path matters during reprogramming. Such discoverability would be unique to this controller because

(Continued on next page)

Biology Box. *Continued*

the intermediate states are not just taken on in passing like in preset overexpression, but rather are sustained in quasi-steady states over time before the next step of mRNA overexpression pushes the cell to the next steady state. As a consequence, while the controlled TFs' concentrations are held constant, the additional TFs in the gene regulatory network have time to stabilize to their corresponding concentrations, which may lead to various cell phenotypes that can be assessed for proximity to pluripotency through gene expression analysis. Accordingly, incremental and sequential up-and-down steady-state perturbations to the controlled TFs may be a promising approach to discover paths to pluripotency (if they exist) in complex steady-state landscapes (see "Discovering Paths to Pluripotency" in the STAR Methods and Figures S3C and S3D).

In summary, the proposed controller has the potential to accurately and quickly steer the concentrations of prescribed TFs to target steady-state values, independent of the endogenous network that regulates these TFs, provided the feedback gain is sufficiently high. It could be useful in applications where one wants to trigger transitions into an existing stable target state, in which case the controller is removed after its task is completed, thus allowing the endogenous TFs to take the concentrations in the target state. It can also be used to stabilize a system to states different from those already present, and as such, it may be useful in metabolic engineering for dynamically optimizing the yield of a product subject to toxicity constraints (Holtz and Keasling, 2010). In this case, the controller should not be removed after task completion as its effort is required to sustain the newly achieved steady-state landscape.

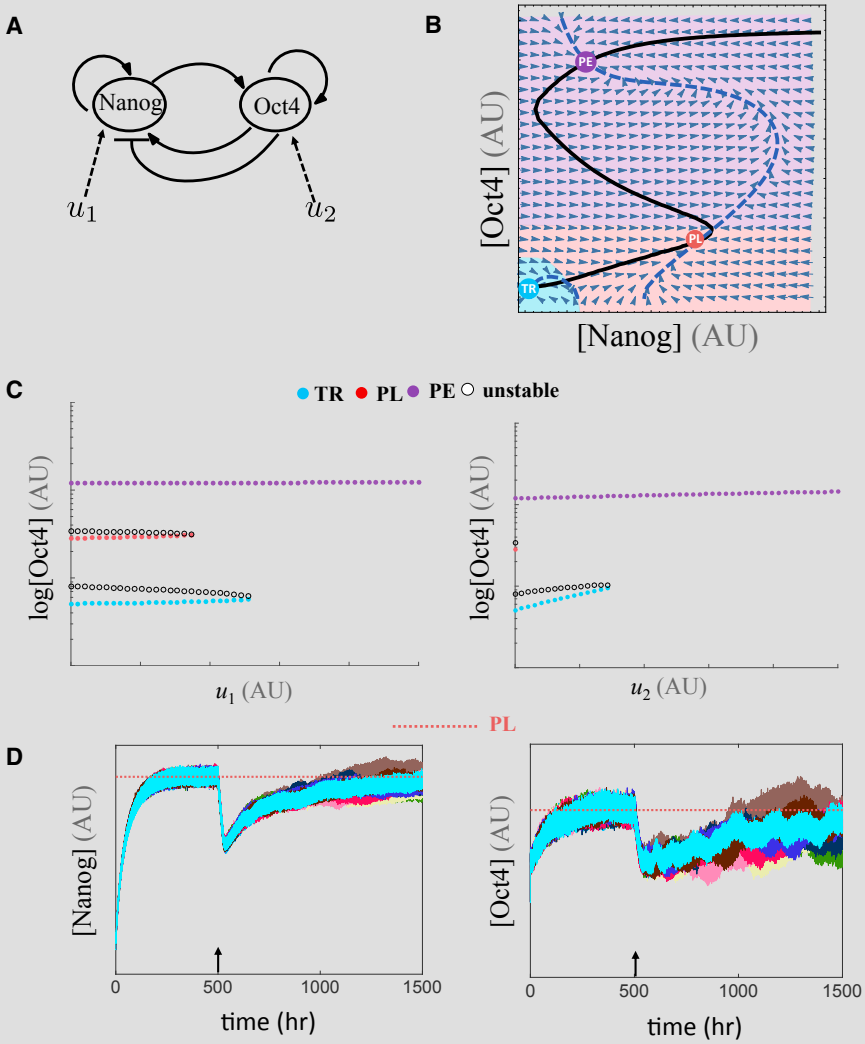

Figure B1. Reprogramming a Network Motif of the Pluripotency Gene Regulatory Network

(A) Two-node network motif with Oct4 and Nanog. Sox2 is lumped with Oct4 because these two TFs often act as a heterodimer (Tapia et al., 2015).

(B) Representative steady-state landscape with three stable steady states: trophectoderm (TR), pluripotent (PL), and primitive endoderm (PE).

(C) Bifurcation diagrams show number, location, and stability of the steady states as u_1 or u_2 increase.

(D) Time traces (10 realizations) of Nanog and Oct4 concentrations while the controller circuit is active (left of arrow) and after shut down (right of arrow). Simulations using the chemical Langevin equation (see "Stochastic Model" in the STAR Methods). Parameters for which preset overexpression fails.

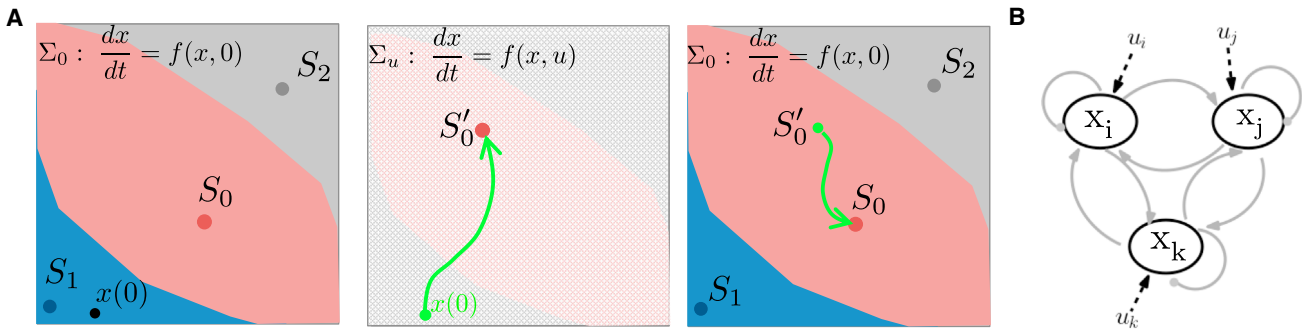

Figure 1. Reprogramming a Multistable Network

(A) Basic idea of reprogramming a system Σ_u to a target state S_0. Colored regions represent different regions of attraction for the states shown, S_0' represents the unique stable steady state following perturbation, and green trace represents the system's trajectory.

(B) Generic cooperative network. The arrowheads on edges represent positive activation and circles represent indeterminate regulation. Only three nodes shown, but an arbitrary number can be present.

have only two stable steady states, $(x_1^a, \ldots, x_n^a)$ and $(x_1^b, \ldots, x_n^b)$, then $(x_1^a, \ldots, x_n^a)$ is maximal if $(x_i^a \geq x_i^b)$ for all $i \in \{1, \ldots, n\}$. Most importantly, a cooperative monotone system with positive perturbation is strongly reprogrammable only to this maximal stable state. It follows that a cooperative network is not strongly reprogrammable to any target state S_0 that is characterized by an intermediate value of any of the TFs concentrations x_i. It is therefore not possible to force all network's states to the region of attraction of an intermediate target state S_0 through preset overexpression. It may be possible, however, to reprogram the system to S_0 if the initial state is lower than it (see "Cooperative Network Reprogramming Properties" in the STAR Methods). However, whether an appropriate level of overexpression exists and, if so, its range, depends critically on the parameters of the Hill functions, as we illustrate in the next example.

Two-Node Cooperative Network Example

Model 1 for the case in which the cooperative network under study has two TFs (Figure 2A) specializes to

$$\Sigma_u : \frac{dx_1}{dt} = H_1(x_1, x_2) - \gamma_1 x_1 + u_1, \frac{dx_2}{dt} = H_2(x_1, x_2) - \gamma_2 x_2 + u_2, H_i(x_1, x_2) = \frac{a_i x_1^2 + b_i x_2^2 + c_i x_1^2 x_2^2}{1 + x_1^2 + x_2^2 + d x_1^2 x_2^2}, i = 1, 2, \quad \text{(Equation 2)}$$

in which we have assumed that the TFs dimerize and cooperate before activating one another and themselves and have normalized the concentrations of the TFs by their respective dissociation constants to reduce the number of parameters. The left-side plot of Figure 2B shows a configuration of the nullclines of system Σ_0 in Equation 2 where $u_1 = u_2 = 0$, which possesses three stable steady states. The plot also depicts the vector field $((dx_1/dt), (dx_2/dt))$, which shows stable and unstable steady states. Based on the regions of attractions shown, for a trajectory to converge to S_0, it must be initialized in the pink region. For all u_1 and u_2 (center and right-side plots of Figure 2B), the perturbed system Σ_u always has a stable steady state in the region of attraction of its maximal steady state S_2 and when the input perturbation is sufficiently large, the system has a unique globally stable steady state in this region. Thus, under extremal perturbation, all trajectories approach this state independently of where they start. Furthermore, when u is set back to zero, the trajectory will ultimately converge to the maximal state S_2, as predicted from theory. By contrast, the system cannot be reprogrammed to the intermediate state S_0 even when initialized at the steady state S_1, which is lower than S_0. In fact, when u_1 and/or u_2 are progressively increased, the equilibrium point near S_0 disappears before the one near S_1 (Figure 2B). Therefore, either the state stays around S_1 for lower overexpression or it switches to S_2 for larger overexpression, leading to failure of reprogramming the system to S_0.

This example illustrates the theoretically predicted difficulty encountered when reprogramming cooperative networks to a state characterized by intermediate values of TF concentrations. This difficulty is conceptually conveyed by the diagram of Figure 2C, in which a ball rolls down through a landscape of valleys under the force of gravity. Let the ball initially be in the S_1 valley when we start pulling up the left-hand side of the landscape. If we pull up too little, the ball will not move from the S_1 valley, as this is still a stable steady configuration (magenta plot). If we pull just enough to make the S_1 valley disappear, the ball will roll out of the S_1 valley but will not land in the S_0 valley, as this valley has also disappeared (cyan plot). That is, when we make the S_1 valley shallow, we also (as a side effect) make the S_0 valley shallow. Hence, the ball rolling out of S_1 misses S_0 regardless of the overexpression level u that is applied.

Taken together, these findings show that in a cooperative network, independently of the number of TFs and the number of stable steady states, excessive overexpression is always a losing strategy for reprogramming the network to an intermediate state. Furthermore, an overexpression level that reprograms a cooperative network to a target intermediate state from a state lower than it, when it exists, may be very narrow and highly sensitive to the network's parameters (see "Cooperative Network Reprogramming Properties" in the STAR Methods). These parameters, in turn, are poorly known and subject to both cell-to-cell and stochastic variability over time, making it practically difficult to appropriately set the overexpression level.

Effect of Additional Regulatory Interactions

The difficulties in reprogramming a cooperative network through preset overexpression of its TFs continue to hold in the presence of additional positive regulatory interactions (type

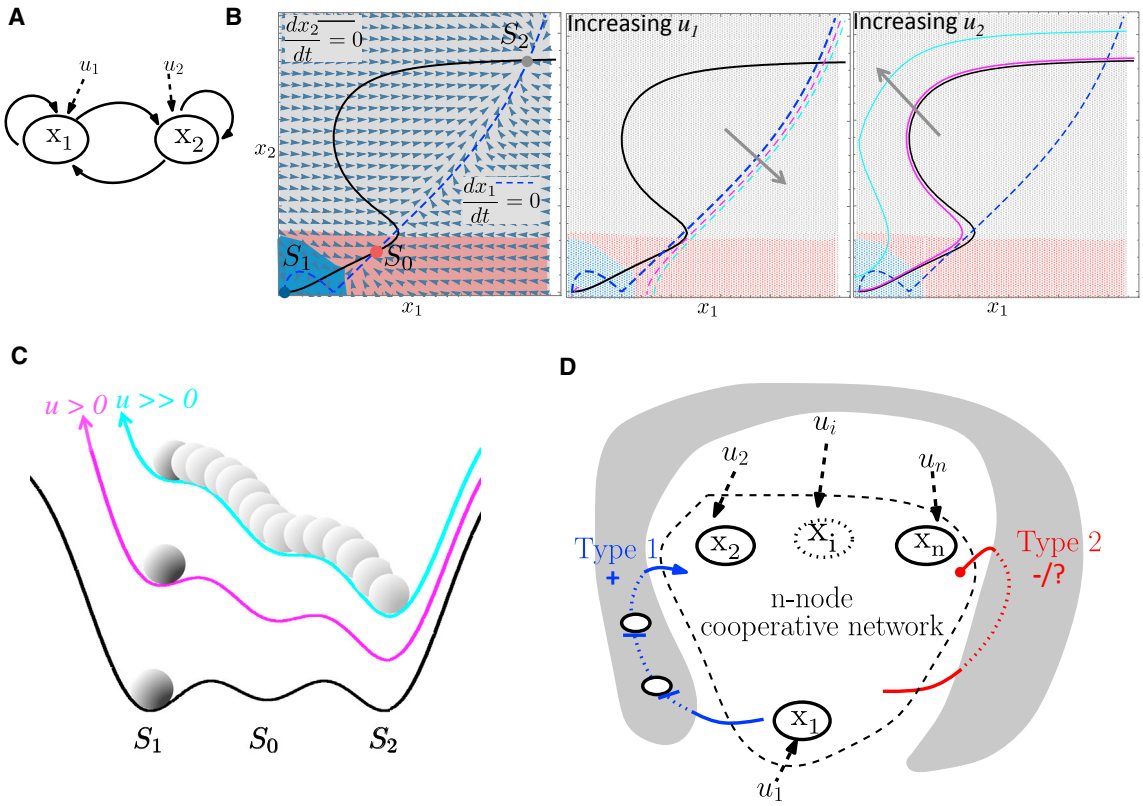

Figure 2. Reprogramming a Cooperative Network

(A) Two-node cooperative network example.

(B) Nullclines ($dx_1/dt = dx_2/dt = 0$) and vector field for the two-node network in (A). Increasing u_1 or u_2 changes the shapes of the $dx_1/dt = 0$ or $dx_2/dt = 0$ nullclines, respectively, such that the intersection in the red region disappears before the intersection in the blue region. Therefore, reprogramming to S_0 is not possible. Parameters are given in "Type 1 Interactions & Reprogramming Properties" in the STAR Methods.

(C) A ball rolling in a valley's landscape under the force of gravity with increasing perturbation.

(D) Type 1 (positive) and type 2 (undetermined or negative) regulatory interactions act as "perturbations" to an *n*-node cooperative network.

1) or of negative/undetermined interactions (type 2), as long as the positive ones dominate. Specifically, we make a distinction between two types of interactions: type 1 and type 2 (Figure 2D). In a type 1 interaction, we have a simple directed path with positive sign resulting from a cascade of activations and repressions that starts from one of the network's TFs and returns to a possibly different network's TF, in which the number of repressions is even. Type 1 interactions do not change the effect of the input perturbations ($u_1,\ldots,u_n$) on the cooperative network's dynamics and therefore do not alter its reprogrammability properties (see "Type 1 Interactions & Reprogramming Properties" in the STAR Methods). The same difficulties exist when attempting to trigger transitions of the network's state x with preset overexpression level u to a configuration where not all network's TF concentrations $x_1,\ldots,x_n$ are maximal. In a type 2 interaction, the directed path that starts from one of the network's TFs and returns to a possibly different network's TF can either be simple and have negative sign or can be undetermined. Type 2 interactions do not necessarily preserve the monotone cooperative structure of the system and hence may lead to different reprogramming outcomes. However, if their effects are dominated by those of the positive regulatory interactions, then there may not exist a preset input level u to trigger transitions of the network's state x to a configuration where not all network's TF concentrations $x_1,\ldots,x_n$ are maximal (see "Type 2 Interactions & Reprogramming Properties" in the STAR Methods).

Reprogramming Gene Networks through Feedback Overexpression

The ability to guarantee desired state transitions through combinations of preset overexpression requires substantial a priori knowledge of the network's structure and parameters. As shown in the previous section, no such combinations of preset overexpression are guaranteed to exist in a cooperative network. When insufficient knowledge of the network is available or the network is known to contain cooperative motifs, alternative overexpression approaches are necessary to guarantee desired state transitions.

Therefore, given a gene regulatory network with n TFs $x_1,\ldots,x_n$ that can each be overexpressed through stimuli $u_1,\ldots,u_n$ (Equation 1), we propose an overexpression strategy that steers the network's state $x = (x_1,\ldots,x_n)$ to any desired state $x^* = (x_1^*,\ldots,x_n^*)$ independently of the network's structure and parameters. This design strategy uses closed loop feedback control, wherein each TF's overexpression level u_i, for $i = 1,\ldots,n$, is

adjusted based on the error between the actual concentration x_i and the desired concentration x_i^*. This approach is in contrast to open loop control, in which the system's input u is a priori fixed at either a constant or time-varying profile (preset) and remains unchanged regardless of the state trajectory. In this sense, the reprogramming approach discussed in the previous section can be regarded as an open loop control strategy.

To illustrate the effect of feedback overexpression, assume that we can directly set $u_i = G_i(x_i^* - x_i)$ with $G_i > 0$ a positive constant. As x_i approaches x_i^* the control effort u_i decreases and reaches zero when $x_i = x_i^*$. If we assume that G_i is sufficiently large such that $G_i x_i >> H_i(x)$ and $G_i >> \gamma_i$, then Equation 1 becomes

$$\frac{dx_i}{dt} = H_i(x) - \gamma_i x_i + G_i\left(x_i^* - x_i\right) \approx G_i\left(x_i^* - x_i\right), \qquad \text{(Equation 3)}$$

from which it follows that $x_i(t)$ will approach its unique steady state, x_i^*, as $t \to \infty$, independent of the regulatory interactions encoded by $H_i(x)$ (how to achieve this precise value by appropriate setting of inducer levels is stated in Equation 6 below). More precisely, we have that $\limsup_{t\to\infty} \left|x_i(t) - x_i^*\right| = (H_M + \gamma_i x_i^*)/(G_i + \gamma_i)$, in which H_M is an upper bound on $H_i(x)$. This is a form of "high-gain feedback control," which has been widely used in many engineering control design problems (Khalil, 2002). As a consequence, the larger the value of G_i, the smaller the error between the steady state of x_i and its prescribed value x_i^*. Furthermore, the convergence rate of $x_i(t)$ to x_i^* increases as G_i increases (see "Properties of High-Gain Negative Feedback" in the STAR Methods). If for every $i \in \{1, \ldots, n\}$ we employ $u_i = G_i(x_i^* - x_i)$, then the state of the network $x(t)$ converges to x^*. If this prescribed state is further chosen to be inside the region of attraction of S_0 and, once $x(t)$ has approached x^*, we set $u_i = 0$ for all $i \in \{1, \ldots, n\}$, then $x(t)$ ultimately converges to S_0. That is, the network is reprogrammed to any desired steady state S_0, independently of the network structure encoded by $H_i(x)$, its parameters, and its initial state.

As an illustrative example, consider again the two-node network of Figure 3A. If G_1 and G_2 are sufficiently large, the nullclines $dx_1/dt = 0$ and $dx_2/dt = 0$ morph into the vertical line going through x_1^* and the horizontal line going through x_2^*, respectively, and intersect at the unique point $x^* = (x_1^*, x_2^*)$. Hence, this is the globally asymptotically stable steady state of the perturbed system, leading all trajectories to converge to x^* regardless of initial conditions. If x^* is in the region of attraction of S_0, the trajectories will approach this state upon shutting down the controller ($u = 0$), leading to reprogramming of the network to S_0 (Figure 3B).

We can qualitatively interpret the stabilizing action of the feedback controller as follows. Because $u_i = G_i x_i^* - G_i x_i$, this control strategy simultaneously applies a large overexpression rate "$G_i x_i^*$" and a similarly large degradation rate "$-G_i x_i$." Qualitatively, the sole application of $u_i = G_i x_i^*$ for all i makes the system's trajectories converge to the region of attraction of the maximal state of Σ_0. By contrast, the sole application of $u_i = -G_i x_i$, for all i makes the system's trajectories converge to the region of attraction of the minimal state of Σ_0. The simultaneous application of these large and opposing forces makes the system's state converge to their "proportion" given by x^*. This interpretation is pictorially represented in Figure 3C using the extended analogy of a ball in a valley landscape.

Implementation of Feedback Overexpression of TF x_i through a Synthetic Genetic Controller Circuit

We implement the high-gain negative feedback overexpression of x_i by simultaneously producing and degrading the mRNA of TF x_i (Figure 3D). In particular, production is achieved by placing a synthetic copy of gene x_i under the control of an inducible promoter with inducer $I_{i,1}$. Degradation of mRNA can be accomplished using a small interfering RNA (siRNA), denoted s_i, with perfect complementarity to both the endogenous and the synthetic mRNA (Carthew and Sontheimer, 2009). The siRNA transcript is induced by $I_{i,2}$ and is encoded along with the synthetic copy of gene x_i on the same DNA. Here, we demonstrate how this circuit steers the total concentration of x_i to a prescribed value x_i^* by using a simple one-step reaction model for the action of siRNA. We then provide simulation results for a more realistic two-step reaction model, discussed in "Synthetic Feedback Controller Circuit" in the STAR Methods.

Referring to the circuit diagram in Figure 3D, we let the inducers activate the target genes through functions $h_{i,j}(\bullet)$, whose specific form is usually of the Michaelis-Menten type (Del Vecchio and Murray, 2014) and is not relevant for the current treatment as long as $h_{i,j}(0) = 0$. We refer to m_i^s and m_i^e as the synthetic and endogenous mRNAs of gene x_i, with x_i^s and x_i^e referring to the resulting proteins, respectively. Because the synthetically encoded gene is identical to the endogenous one, they effectively encode the same mRNAs and proteins and therefore $m_i = m_i^e + m_i^s$ and $x_i = x_i^e + x_i^s$ (with m_i and x_i referring to the mRNA and protein of gene x_i). Keeping track of endogenous and synthetic species separately, we can write the reactions of the system as

reactions affecting endogenous species:

$$\varnothing \xrightarrow{\overline{H}_i(x)} m_i^e, m_i^e \xrightarrow{\delta_i} \varnothing, m_i^e + s_i \xrightarrow{\overline{k}_i} s_i, m_i^e \xrightarrow{k_i} x_i^e, x_i^e \xrightarrow{\gamma_i} \varnothing,$$

and reactions affecting synthetic species:

$$\varnothing \xrightarrow{Dh_{i,1}(I_{i,1})} m_i^s, m_i^s \xrightarrow{\delta_i} \varnothing, m_i^s + s_i \xrightarrow{\overline{k}_i} s_i, m_i^s \xrightarrow{k_i} x_i^s, x_i^s \xrightarrow{\gamma_i} \varnothing$$

$$\varnothing \xrightarrow{Dh_{i,2}(I_{i,2})} s_i, s_i \xrightarrow{\beta_i} \varnothing.$$

With δ_i and γ_i, we model decay of mRNA and protein, respectively, due to dilution and degradation, while with β_i, we model dilution due to cell growth. Because siRNA is stable, we assume it is only affected by dilution (Carthew and Sontheimer, 2009). Let $\alpha_i = h_{i,2}(I_{i,2})$ and assume that siRNA is induced sufficiently earlier than the mRNA species so that its concentration reaches a proximity of the equilibrium $s_i^* = D\alpha_i/\beta_i$ by the time the mRNA species are expressed. This assumption simplifies the analysis, but the stability properties of the system hold independent of this simplification. The ODE model describing the endogenous and synthetic species' concentrations becomes

$$\frac{dm_i^e}{dt} = \overline{H}_i(x) - \delta m_i^e - \overline{k}_i s_i^* m_i^e, \quad \frac{dx_i^e}{dt} = k_i m_i^e - \gamma_i x_i^e, \qquad \text{(Equation 4)}$$

$$\frac{dm_i^s}{dt} = Dh_{i,1}(I_{i,1}) - \delta m_i^s - \overline{k}_i s_i^* m_i^s, \quad \frac{dx_i^s}{dt} = k_i m_i^s - \gamma_i x_i^s, \qquad \text{(Equation 5)}$$

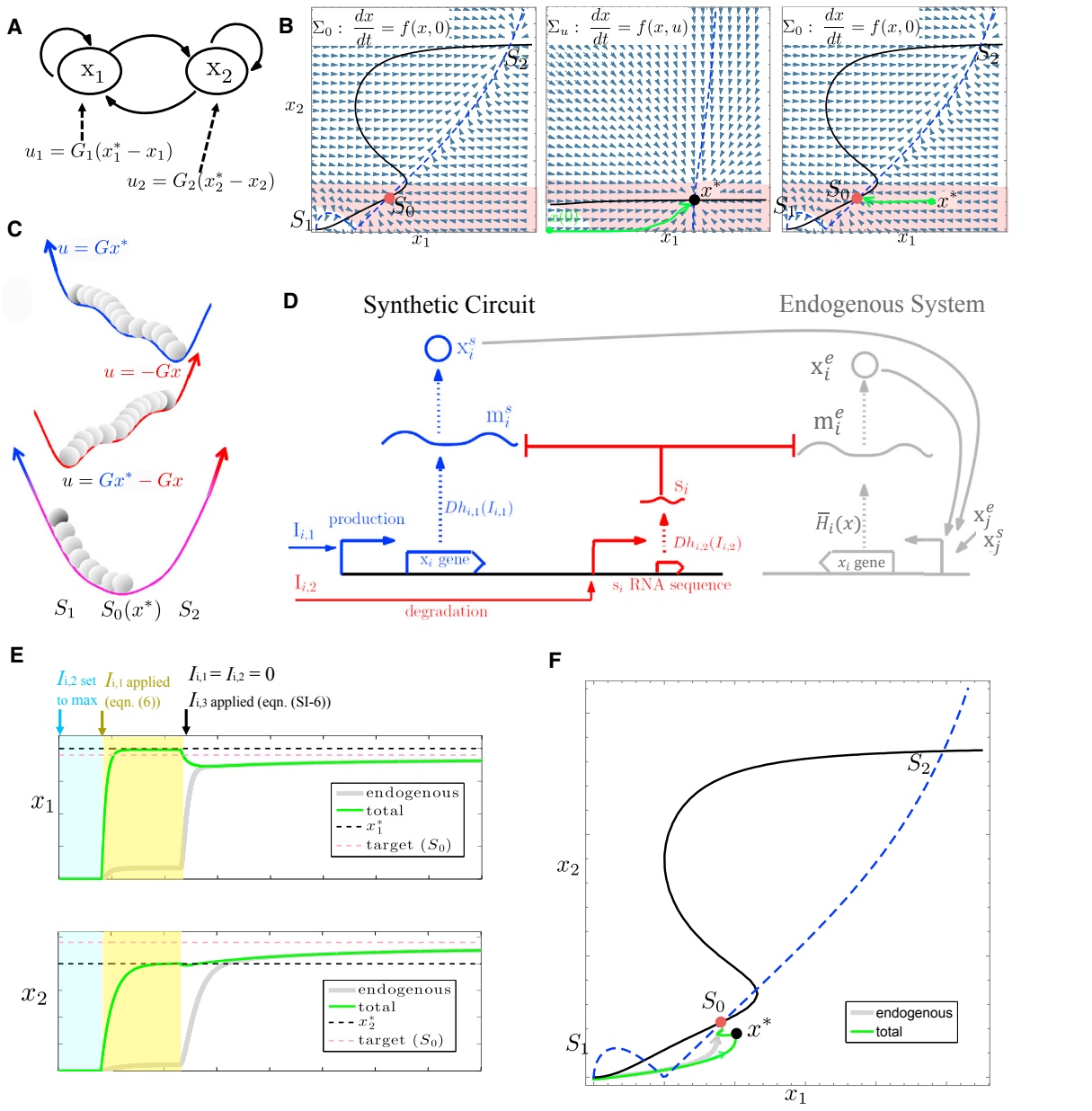

Figure 3. Reprogramming Gene Regulatory Network via Feedback Overexpression

(A) Two-node cooperative network with feedback overexpression of TFs.

(B) High-gain feedback makes the network monostable at the target state x^*, located in the pink region of attraction of target state S_0.

(C) Pictorial representation of the effect of high-gain negative feedback input on a valley landscape (compare to Figure 1E).

(D) Synthetic genetic controller circuit that implements feedback overexpression of TF x_i. Species x_i^e, m_i^e, x_i^s, m_i^s represent endogenous TF and mRNA, synthetic TF, and mRNA, respectively. $I_{i,1}$ and $I_{i,2}$ are inducers, and s_i is siRNA targeting m_i^e and m_i^s.

(E) Time traces of total TF concentrations x_1 and x_2 (corresponding to the network of A), where each TF is controlled by a copy of the circuit in (D).

(F) Trajectories in (x_1,x_2) plane corresponding to time traces of (E) and nullclines of network in (A). Parameters equivalent to those of Figure 1 (listed in Table S1), for which it is not possible to transition to S_0 with preset overexpression.

in which D is the concentration of the circuit's DNA and $\overline{H}_i(x) = (\delta_i/\kappa_i)H_i(x)$, with $H_i(x)$ being the Hill function introduced previously when mRNA dynamics were assumed at their quasi-steady state.

Let x_i^* be the prescribed concentration to which we want to steer TF x_i and let $m_i^* = (\gamma_i/\kappa_i)x_i^*$ be its corresponding steady state mRNA concentration. Then, using inducer concentration $I_{i,1}^*$ such that

$$\frac{\kappa_i}{\gamma_i}\frac{\beta_i h_{i,1}\left(I_{i,1}^*\right)}{\overline{k}_i\alpha_i} = x_i^* \Rightarrow I_{i,1}^* = h_{i,1}^{-1}\left(x_i^*\frac{\gamma_i\overline{k}_i\alpha_i}{\kappa_i\beta_i}\right), \qquad \text{(Equation 6)}$$

and adding the left and right-hand sides of Equations 4 and 5, we obtain the ODEs for the total species concentrations:

$$\frac{dm_i}{dt} = \overline{H}_i(x) - \delta_i m_i + G_i\left(m_i^* - m_i\right), \quad \frac{dx_i}{dt} = \kappa_i m_i - \gamma_i x_i, \quad G_i = D\frac{\overline{k}_i \alpha_i}{\beta_i}. \tag{Equation 7}$$

It follows from this that if G_i is sufficiently large such that $G_i m_i^* >> \overline{H}_i(x)$ and $G_i >> \delta_i$, then we have that $(dm_i/dt) \approx G_i(m_i^* - m_i)$, and therefore $m_i(t) \rightarrow m_i^*$ and $x_i(t) \rightarrow x_i^*$ as $t \rightarrow \infty$, leading to convergence of the total TF's concentration x_i to the prescribed value x_i^*. Concurrently, the endogenous TF concentration $x_i^e(t)$ approaches a small value, due to enhanced degradation by the siRNA (Equation 4), while the synthetic TF's concentration $x_i^s(t)$ approaches the proximity of the prescribed value x_i^* (Equation 5). Thus, the net effect of the synthetic genetic circuit is to bring the total concentration of the TF x_i to x_i^* by supplying this concentration with the synthetically produced TF and concurrently degrading the endogenously produced TF. Note that a major difference with the ideal feedback overexpression model in Equation 3 is that the negative feedback is applied to the mRNA's concentration and not to the TF's concentration directly. Therefore, while we can substantially speed up the transcription process with increased G_i, the translation speed remains unchanged. These results remain qualitatively unchanged if a more realistic two-step reaction model for the siRNA reaction is considered (Haley and Zamore, 2004; Cuccato et al., 2011):

$$m_i^k + s_i \underset{d_i}{\overset{a_i}{\rightleftharpoons}} c_i^k \xrightarrow{k_i} s_i, \quad c_i^k \xrightarrow{\beta_i} \varnothing, \quad k \in \{e, s\},$$

which leads to the new ODE model for the total concentrations m_i and x_i:

$$\frac{ds_i}{dt} = Dh_{i,2}(I_{i,2}) - \beta_i s_i - a_i m_i s_i + (d_i + k_i)c_i,$$

$$\frac{dc_i}{dt} = a_i m_i s_i - (d_i + k_i)c_i - \beta_i c_i$$

$$\frac{dm_i}{dt} = \overline{H}_i(x) - \delta_i m_i + Dh_{i,1}(I_{i,1}) - a_i m_i s_i + d_i c_i, \qquad \frac{dx_i}{dt} = k_i m_i - \gamma_i x_i. \tag{Equation 8}$$

This system can be taken to a form similar to Equation 7 using quasi-steady state approximations of the enzymatic reactions along with the assumption $m_i << K_M$, with $K_M = (d_i + k_i)/\alpha_i$ the Michaelis-Menten constant of the siRNA reaction. This inequality is satisfied for physiologically relevant values of the mRNA concentration (Haley and Zamore, 2004) and therefore through the operation of the controller if overexpression of mRNA is applied sufficiently after siRNA has been overexpressed. Accordingly, the level of the inducer $I_{i,1}^*$ that results in the prescribed concentration x_i^* and the expression of the gain G_i are the same as those in Equations 6 and 7, respectively, in which $\overline{k}_i = k_i/K_M$. Therefore, we will have that $m_i(t) \rightarrow m_i^*$ and $x_i(t) \rightarrow x_i^*$ as $t \rightarrow \infty$, as before (see "Synthetic Feedback Controller Circuit" in the STAR Methods).

In summary, the requirements for the controller to steer the concentration x_i to its prescribed value x_i^* are: (1) $G_i >> \delta_i$ and $G_i m_i^* \gg \overline{H}_i(x)$ (large gain), and (2) $m_i << K_M$ (mRNA does not saturate the siRNA). While the second requirement can be easily guaranteed by keeping the mRNA's concentration within physiological ranges, the first requirement must be engineered in the controller by having a sufficiently large DNA copy number D (expression of G_i in Equation 7). In "Synthetic Genetic Feedback Controller Circuit" in the STAR Methods, we estimate that a few copies of synthetic circuit DNA D suffices to realize a large gain G_i, based on physiological values of mRNA concentrations and decay rates in mammalian cells. When requirements (1) and (2) are ensured, the specific values of the species concentration are not relevant for the proper functioning of the controller, and thus we have used arbitrary units for the simulations.

Figure 3E shows simulation results for the system in Equation 8 with $i \in \{1,2\}$ for the case in which TFs x_1 and x_2 of the two-node gene regulatory network of Figure 3A are each being controlled by a copy of the controller of Figure 3D. The specific parameters chosen for the gene regulatory network are the same as those of Figure 2B, in which preset overexpression failed to reprogram the system to S_0 in all cases. In the simulations, the controller is active during the time interval marked by the yellow area in Figure 3E. During this time, the controller quickly steers the TFs' concentrations to their prescribed values x_1^* and x_2^*, as expected from theory. The impact of decreasing G_i on the circuit's performance is illustrated in Figure S2A. In addition, Figure S2B shows that the controller circuit successfully steers x_1 and x_2 to the prescribed values even when the initial state of the network $(m(0),x(0))$, with $m = (m_1, m_2)$ and $x = (x_1, x_2)$, is in the region of attraction of the highest stable state S_2 (that was impossible to escape from with preset overexpression). This is expected from theory given that the controller can steer the network to the prescribed state independently of the initial condition.

Reprogramming Gene Networks with the Synthetic Genetic Controller Circuit

Let $S_0 = (m^{S_0}, x^{S_0})$ be the target stable steady state of the endogenous network

$$\frac{dm_i}{dt} = \overline{H}_i(x) - \delta_i m_i, \quad \frac{dx_i}{dt} = k_i m_i - \gamma_i x_i, \quad i = 1, \ldots, n, \tag{Equation 9}$$

where $x_i^{S_0}$ is the concentration of TF x_i in S_0 and $m_i^{S_0} = (\gamma_i/\kappa_i)x_i^{S_0}$ is the corresponding mRNA concentration. We implement the synthetic genetic circuit of Figure 3D for each of the network's TFs x_i and select the prescribed value x_i^* so that the resulting network state (m^*, x^*) is in the region of attraction of the target state S_0 and possibly close to it. Therefore, Equation 9 is modified to the closed loop system in Equation 8 for $i \in \{1,\ldots, n\}$. By the results of the previous section, the genetic circuit steers the total concentrations m_i and x_i to m_i^* and x_i^*, respectively, for all $i \in \{1,\ldots, n\}$, by supplying m_i^s and x_i^s while actively degrading the endogenous mRNA. Because the genetic circuit holds x at x^*, the endogenous mRNAs are produced at a rate determined by the Hill functions evaluated at x^*, that is, $\overline{H}_i(x^*)$ (Equation 4). These production rates, in turn, are close to what we have in the target stable state S_0 because x^* is close to x^{S0}. This fact allows the endogenous system to take over the synthetic circuit and to supply the TFs' concentrations found in S_0 once the controller is shut down.

We can mathematically formulate this behavior as follows. Assume that the controller can be shut down instantaneously, that

is, we can set $I_{i,1} = I_{i,2} = s_i = c_i = 0$ for all $i \in \{1,\ldots, n\}$ in Equation 8 (“Feedback Controller Shutdown” in the STAR Methods analyzes the case where s_i and c_i take time to decay). This leads to new ODEs for the total species concentration:

$$\frac{dm_i}{dt} = \overline{H}_i(x) - \delta_i m_i, \quad \frac{dx_i}{dt} = k_i m_i - \gamma_i x_i, \text{ with } m_i(0) = m_i^*, x_i(0) = x_i^*, i = 1, \ldots, n. \quad \text{(Equation 10)}$$

Because the initial condition (m^*, x^*) of this system is in the region of attraction of the target state S_0, we have that $x(t) \to x^{S_0}$ as $t \to \infty$. The ODE model of the synthetic species concentrations is given by

$$\frac{dm_i}{dt} = \overline{H}_i(x) - \delta_i m_i, \quad \frac{dx_i^s}{dt} = k_i m_i^s - \gamma_i x_i^s, \text{ with } m_i^s(0) \approx m_i^*, \; x_i^s(0) \approx x_i^*, i = 1, \ldots, n,$$

leading to $x_i^s(t) \to 0$ as $t \to \infty$. Because $x_i^e(t) = x_i(t) - x_i^s(t)$, we must have that $x_i^e(t) \to x_i(t)$ as $t \to \infty$. This implies that $x_i^e(t) \to x_i^{S_0}$ as $t \to \infty$ for all $i \in \{1,\ldots, n\}$. That is, the endogenously produced TFs compensate for the decaying concentrations of the synthetic TFs and ultimately “lock” into the concentration found in the target state S_0. This is shown in the simulation results of Figure 3E, in which the controller is shut down at the time indicated by the second arrow. The system simulated after the shutdown is in Equations S1, S2, S3, S4, S5, S6, and S7, in which we have included siRNA sponges to speed up the removal of siRNA upon setting $I_{i,1} = I_{i,2} = 0$ for each i.

In the simulations, the endogenous network is the two-node gene regulatory network of Figure 3A. The parameters of the Hill functions $\overline{H}_i(x)$ for $i \in \{1,2\}$ are such that open loop overexpression fails to trigger transitions into S_0 (see Figure 2B). Both the total concentrations x_1 and x_2 and the endogenous concentrations x_1^e and x_2^e are shown. By the end of the time marked by the yellow shaded area, $x_1(t)$ and $x_2(t)$ have reached their prescribed values x_1^* and x_2^*, selected in the proximity of $x_1^{S_0}$ and $x_2^{S_0}$, respectively. At this time, we set $I_{i,1} = 0$ and $I_{i,2} = 0$ for $i \in \{1,2\}$ and overexpress the sponges. The plots show that the total TFs’ concentration, after a transient decrease due to the initial presence of siRNA, converge to the target values $x_1^{S_0}$ and $x_2^{S_0}$. In particular, after the controller is shut down, the endogenous species concentration x_1^e and x_2^e converge to the total concentrations x_1 and x_2, and finally to the values characterizing the target state S_0. The corresponding trajectories in the (x_1, x_2) plane during the entire process are illustrated in Figure 3F superimposed to the nullclines of the endogenous network.

In summary, the controlled network is a monostable system in which the enforced unique stable steady state has TFs concentrations x_1^* and x_2^* prescribed by the inducers $I_{1,1}^*$ and $I_{2,1}^*$ in Equation 6. Once the controlled network’s state has reached the prescribed concentrations of the TFs, the controller is shut down by setting the inducer levels back to zero (and by adding sponges if required to speed up the process). Therefore, the synthetic TFs concentrations x_1^s and x_2^s decay to zero while the endogenous ones x_1^e and x_2^e reach the total TFs’ concentrations x_1 and x_2, which are, in turn, approaching their concentrations in the target state S_0, leading to reprogramming the endogenous network to S_0.

DISCUSSION

Using preset overexpression levels of TFs to trigger desired transitions in multistable gene regulatory networks is an experimentally convenient approach. However, its efficacy heavily relies on the specific dynamical properties of the network. In particular, when the gene regulatory network is cooperative, we have shown that preset overexpression of TFs may be insufficient to trigger certain state transitions. To tackle this problem, we have proposed a synthetic genetic controller circuit that implements feedback overexpression of the network’s TFs, wherein the expression level is adjusted based on the discrepancy between the actual and desired TF’s concentration. This genetic circuit has the capability to steer the concentration of the controlled TFs to any desired value, independently of the network’s structure and parameters, provided the feedback gain is sufficiently high. When applied to control all of the network’s TFs, this approach allows for the triggering of arbitrary state transitions in any multistable gene regulatory network.

A number of practical considerations are relevant for implementation of the controller in living cells. First, the high gain conditions assumed throughout must be satisfied, for example through a sufficiently high copy number of the DNA carrying the controller components. Because our calculations suggest that a copy number equal to 1 should be sufficient, integrating approaches using lentiviral transfection (Warlich et al., 2011) could realize the high-gain condition. In applications where genomic integration is undesirable, alternative delivery mechanisms may be considered such as Epstein-Barr-derived episomal vectors that replicate at most once per cell cycle (Yates and Guan, 1991). In this case, the effects of copy number variability on the controller performance should be investigated. The second condition to ensure is that the mRNA of the species under control does not saturate the siRNA, that is, m_i remains small compared to the Michaelis-Menten constant of the siRNA binding reaction ($m_i << K_M$) a constraint that should generally be satisfied in physiological conditions (Haley and Zamore, 2004). Finally, for cell fate reprogramming, it is important that upon controller shutdown, the controller species are removed sufficiently fast to avoid destabilizing the target state reached (see “Synthetic Feedback Controller Circuit” in the STAR Methods).

The high-gain feedback control strategy that we have proposed is one possibility for robust set point control. Other options include integral feedback, as proposed in Briat et al. (2016a) for certain classes of systems. However, such integral feedback designs assume that species do not dilute (i.e., no cell growth), making them better suited for reconstituted cell-free systems (an elegant realization of this has been proposed in Briat et al., [2016b]). Interestingly, the mathematical formulation of integral control of Briat et al. (2016a) requires that the “control input” on the target’s equation is an additive positive perturbation, leading to the same shortcomings as preset overexpression for the gene regulatory network reprogramming problem of this paper.

The blueprint of the controller we have presented, which is capable of robust stabilization of TF concentrations in endogenous gene regulatory networks is a new synthetic biology design to the best of our knowledge. Furthermore, while the inner/outer loop control scheme we have proposed is common in many

engineering applications to decouple the control of different variables (Murray, 2008), its biological realization is novel in synthetic biology. This nested-loop control scheme may prove valuable in complementing in silico feedback control approaches and, more generally, may serve applications where accurate tuning of TFs' steady state concentrations is of interest.

STAR★METHODS

Detailed methods are provided in the online version of this paper and include the following:

- KEY RESOURCES TABLE
- CONTACT FOR REAGENT AND RESOURCE SHARING
- METHOD DETAILS
  - Cooperative Network Reprogramming Properties
  - Type 1 Interactions and Reprogramming Properties
  - Type 2 Interactions and Reprogramming Properties
  - Properties of High-Gain Negative Feedback
  - Synthetic Feedback Controller Circuit
  - Outer Loop Feedback Control for Adjusting x_i^*
  - Discovering Paths to Pluripotency
  - High Gain and Noise in the Genetic Controller
  - Stochastic Model
  - Published Models of the Pluripotent Network

SUPPLEMENTAL INFORMATION

Supplemental Information includes four figures, three tables, and one data file and can be found with this article online at http://dx.doi.org/10.1016/j.cels.2016.12.001.

AUTHOR CONTRIBUTIONS

D.D.V. designed the research, performed mathematical analysis, and wrote the manuscript. H.A. performed simulations and assisted in writing manuscript. Y.Q. assisted in simulations. J.J.C. designed the research and edited the manuscript.

ACKNOWLEDGMENTS

The authors would like to thank Prof. Eduardo Sontag and Prof. Ron Weiss for discussions on the monotone cooperative nature of the pluripotency network and on the siRNA technology for the implementation of the feedback controller, respectively. The authors would also like to thank Prof. George Daley for a number of useful discussions both on the reprogrammability property of the pluripotency network and on the feedback controller concept. Finally, the authors would like to thank Ms. Narmada Herath for technical support with the stochastic analysis. This work was supported in part by NIGMS grant P50 GMO98792.

SUPPORTING CITATIONS

The following references appear in the Supplemental Information: Muñoz Descalzo et al. (2013); Siwiak and Zielenkiewicz (2013).

Received: April 8, 2016
Revised: July 18, 2016
Accepted: December 1, 2016
Published: January 5, 2017

REFERENCES

Alon, U. (2007). An Introduction to Systems Biology. Design Principles of Biological Circuits (Boca Raton, FL: Chapman-Hall/CRC).

Angeli, D., and Sontag, E. (2003). Monotone control systems. IEEE Trans. Automat. Contr. *48*, 1684–1698.

Ariyur, K.B., and Krstic, M. (2003). Real-Time Optimization by Extremum-Seeking Control (Hoboken, NJ: Wiley).

Boyer, L.A., Lee, T.I., Cole, M.F., Johnstone, S.E., Levine, S.S., Zucker, J.P., Guenther, M.G., Kumar, R.M., Murray, H.L., Jenner, R.G., et al. (2005). Core transcriptional regulatory circuitry in human embryonic stem cells. Cell *122*, 947–956.

Briat, C., Gupta, A., and Khammash, M. (2016a). Antithetic integral feedback ensures robust perfect adaptation in noisy biomolecular networks. Cell Syst. *2*, 15–26.

Briat, C., Zechner, C., and Khammash, M. (2016b). Design of a synthetic integral feedback circuit: dynamic analysis and DNA implementation. ACS Synth. Biol. *5*, 1108–1116.

Cahan, P., and Daley, G.Q. (2013). Origins and implications of pluripotent stem cell variability and heterogeneity. Nat. Rev. Mol. Cell Biol. *14*, 357–368.

Carey, B.W., Markoulaki, S., Hanna, J.H., Faddah, D.A., Buganim, Y., Kim, J., Ganz, K., Steine, E.J., Cassady, J.P., Creyghton, M.P., et al. (2011). Reprogramming factor stoichiometry influences the epigenetic state and biological properties of induced pluripotent stem cells. Cell Stem Cell *9*, 588–598.

Carthew, R.W., and Sontheimer, E.J. (2009). Origins and mechanisms of miRNAs and siRNAs. Cell *136*, 642–655.

Chambers, I., Colby, D., Robertson, M., Nichols, J., Lee, S., Tweedie, S., and Smith, A. (2003). Functional expression cloning of Nanog, a pluripotency sustaining factor in embryonic stem cells. Cell *113*, 643–655.

Chickarmane, V., and Peterson, C. (2008). A computational model for understanding stem cell, trophectoderm and endoderm lineage determination. PLoS ONE *3*, e3478.

Chickarmane, V., Troein, C., Nuber, U.A., Sauro, H.M., and Peterson, C. (2006). Transcriptional dynamics of the embryonic stem cell switch. PLoS Comput. Biol. *2*, e123.

Cuccato, G., Polynikis, A., Siciliano, V., Graziano, M., di Bernardo, M., and di Bernardo, D. (2011). Modeling RNA interference in mammalian cells. BMC Syst. Biol. *5*, 19.

Darzacq, X., Shav-Tal, Y., de Turris, V., Brody, Y., Shenoy, S.M., Phair, R.D., and Singer, R.H. (2007). In vivo dynamics of RNA polymerase II transcription. Nat. Struct. Mol. Biol. *14*, 796–806.

Davey, B.A., and Priestley, H.A. (2002). Introduction to Lattices and Order (New York: Cambridge University Press).

Del Vecchio, D., and Murray, R.M. (2014). Biomolecular Feedback Systems (Princeton: Princeton University Press).

Del Vecchio, D., and Slotine, J.J. (2013). A contraction theory approach to singularly perturbed systems. IEEE Trans. Automat. Contr. *58*, 752–757.

Ebert, M.S., Neilson, J.R., and Sharp, P.A. (2007). MicroRNA sponges: Competitive inhibitors of small RNAs in mammalian cells. Nat Methods *4*, 721–726.

Faucon, P.C., Pardee, K., Kumar, R.M., Li, H., Loh, Y.H., and Wang, X. (2014). Gene networks of fully connected triads with complete auto-activation enable multistability and stepwise stochastic transitions. PLoS ONE *9*, e102873.

Feng, H., and Wang, J. (2012). A new mechanism of stem cell differentiation through slow binding/unbinding of regulators to genes. Sci. Rep. *2*, 550.

Gillespie, D.T. (2000). The chemical Langevin equation. J. Chem. Phys. *113*, 297–306.

Goh, P.A., Caxaria, S., Casper, C., Rosales, C., Warner, T.T., Coffey, P.J., and Nathwani, A.C. (2013). A systematic evaluation of integration free reprogramming methods for deriving clinically relevant patient specific induced pluripotent stem (iPS) cells. PLoS ONE *8*, e81622.

Graf, T., and Enver, T. (2009). Forcing cells to change lineages. Nat. Rev. *462*, 587–594.

Haley, B., and Zamore, P.D. (2004). Kinetic analysis of the RNAi enzyme complex. Nat. Struct. Mol. Biol. *11*, 599–606.

Hanna, J., Saha, K., Pando, B., van Zon, J., Lengner, C.J., Creyghton, M.P., van Oudenaarden, A., and Jaenisch, R. (2009). Direct cell reprogramming is a stochastic process amenable to acceleration. Nature *462*, 595–601.

Hanna, J.H., Saha, K., and Jaenisch, R. (2010). Pluripotency and cellular reprogramming: facts, hypotheses, unresolved issues. Cell *143*, 508–525.

Herberg, M., Kalkan, T., Glauche, I., Smith, A., and Roeder, I. (2014). A model-based analysis of culture-dependent phenotypes of mESCs. PLoS ONE *9*, e92496.

Holtz, W.J., and Keasling, J.D. (2010). Engineering static and dynamic control of synthetic pathways. Cell *140*, 19–23.

Huang, S. (2009). Reprogramming cell fates: reconciling rarity with robustness. BioEssays *31*, 546–560.

Jaenisch, R., and Young, R. (2008). Stem cells, the molecular circuitry of pluripotency and nuclear reprogramming. Cell *132*, 567–582.

Jens, M., and Rajewsky, N. (2015). Competition between target sites of regulators shapes post-transcriptional gene regulation. Nat. Rev. Genet. *16*, 113–126.

Kalmar, T., Lim, C., Hayward, P., Muñoz-Descalzo, S., Nichols, J., Garcia-Ojalvo, J., and Martinez Arias, A. (2009). Regulated fluctuations in nanog expression mediate cell fate decisions in embryonic stem cells. PLoS Biol. *7*, e1000149.

Khalil, H. (2002). Nonlinear Systems (Upper Saddle River: Prentice Hall).

Kim, J., Chu, J., Shen, X., Wang, J., and Orkin, S.H. (2008). An extended transcriptional network for pluripotency of embryonic stem cells. Cell *132*, 1049–1061.

Kloeden, P.E., and Platen, E. (1992). Numerical Solution of Stochastic Differential Equations (New York: Springer).

Li, C., and Wang, J. (2013). Quantifying cell fate decisions for differentiation and reprogramming of a human stem cell network: landscape and biological paths. PLoS Comput. Biol. *9*, e1003165.

Menolascina, F., Fiore, G., Orabona, E., De Stefano, L., Ferry, M., Hasty, J., di Bernardo, M., and di Bernardo, D. (2014). In-vivo real-time control of protein expression from endogenous and synthetic gene networks. PLoS Comput. Biol. *10*, e1003625.

Milias-Argeitis, A., Summers, S., Stewart-Ornstein, J., Zuleta, I., Pincus, D., El-Samad, H., Khammash, M., and Lygeros, J. (2011). In silico feedback for in vivo regulation of a gene expression circuit. Nat Biotechnol. *29*, 1114–1116.

Milo, R., Jorgensen, P., Moran, U., Weber, G., and Springer, M. (2010). BioNumbers—the database of key numbers in molecular and cell biology. Nucleic Acids Res. *38*, D750–D753.

Morris, S.A., and Daley, G.Q. (2013). A blueprint for engineering cell fate: current technologies to reprogram cell identity. Cell Res. *23*, 33–48.

Muñoz Descalzo, S., Rué, P., Faunes, F., Hayward, P., Jakt, L.M., Balayo, T., Garcia-Ojalvo, J., and Martinez Arias, A. (2013). A competitive protein interaction network buffers Oct4-mediated differentiation to promote pluripotency in embryonic stem cells. Mol. Syst. Biol. *9*, 694.

Mullin, N.P., Yates, A., Rowe, A.J., Nijmeijer, B., Colby, D., Barlow, P.N., Walkinshaw, M.D., and Chambers, I. (2008). The pluripotency rheostat Nanog functions as a dimer. Biochem. J. *411*, 227–231.

Murray, R.M. (2008). Feedback Systems: An Introduction for Scientists and Engineers (Princeton, NJ: Princeton University Press).

Niaken, K.K., Ji, H., Maehr, R., Vokes, S.A., Rodolfa, K.T., Sherwood, R.I., Yamaki, M., Dimos, J.T., Chen, A.E., Melton, D.A., et al. (2010). Sox17 promotes differentiation in mouse embryonic stem cells by directly regulating extraembryonic gene expression and indirectly antagonizing self-renewal. Genes Dev. *24*, 312–326.

Nikolaev, E.V., and Sontag, E.D. (2016). Quorum-sensing synchronization of synthetic toggle switches: A design based on monotone dynamical systems theory. PLoS Comput. Biol. *12*, e1004881.

Niwa, H., Miyazaki, J., and Smith, A.G. (2000). Quantitative expression of Oct-3/4 defines differentiation, dedifferentiation or self-renewal of ES cells. Nat. Genet. *24*, 372–376.

Niwa, H., Toyooka, Y., Shimosato, D., Strumpf, D., Takahashi, K., Yagi, R., and Rossant, J. (2005). Interaction between Oct3/4 and Cdx2 determines trophectoderm differentiation. Cell *123*, 917–929.

Nocedal, J., and Wright, S. (2000). Numerical Optimization (New York: Springer).

Palmieri, S.L., Peter, W., Hess, H., and Schöler, H.R. (1994). Oct-4 transcription factor is differentially expressed in the mouse embryo during establishment of the first two extraembryonic cell lineages involved in implantation. Dev. Biol. *166*, 259–267.

Radzisheuskaya, A., Chia, Gle.B., dos Santos, R.L., Theunissen, T.W., Castro, L.F.C., Nichols, J., and Silva, J.C.R. (2013). A defined Oct4 level governs cell state transitions of pluripotency entry and differentiation into all embryonic lineages. Nat. Cell Biol. *15*, 579–590.

Schlaeger, T.M., Daheron, L., Brickler, T.R., Entwisle, S., Chan, K., Cianci, A., DeVine, A., Ettenger, A., Fitzgerald, K., Godfrey, M., et al. (2015). A comparison of non-integrating reprogramming methods. Nat. Biotechnol. *33*, 58–63.

Schwanhäusser, B., Busse, D., Li, N., Dittmar, G., Schuchhardt, J., Wolf, J., Chen, W., and Selbach, M. (2011). Global quantification of mammalian gene expression control. Nature *473*, 337–342.

Sharova, L.V., Sharov, A.A., Nedorezov, T., Piao, Y., Shaik, N., and Ko, M.S. (2009). Database for mRNA half-life of 19 977 genes obtained by DNA microarray analysis of pluripotent and differentiating mouse embryonic stem cells. DNA Res. *16*, 45–58.

Shu, J., Wu, C., Wu, Y., Li, Z., Shao, S., Zhao, W., Tang, X., Yang, H., Shen, L., Zuo, X., et al. (2013). Induction of pluripotency in mouse somatic cells with lineage specifiers. Cell *153*, 963–975.

Siwiak, M., and Zielenkiewicz, P. (2013). Transimulation - protein biosynthesis web service. PLoS ONE *8*, e73943.

Smith, H.L. (1995). Monotone Dynamical Systems: An Introduction to the Theory of Competitive and Cooperative Systems (Providence: American Mathematical Society).

Soufi, A., Donahue, G., and Zaret, K.S. (2012). Facilitators and impediments of the pluripotency reprogramming factors' initial engagement with the genome. Cell *151*, 994–1004.

Takahashi, K., and Yamanaka, S. (2006). Induction of pluripotent stem cells from mouse embryonic and adult fibroblast cultures by defined factors. Cell *126*, 663–676.

Takahashi, K., and Yamanaka, S. (2016). A decade of transcription factor-mediated reprogramming to pluripotency. Nat. Rev. Mol. Cell Biol. *17*, 183–193.

Tapia, N., MacCarthy, C., Esch, D., Gabriele Marthaler, A., Tiemann, U., Araúzo-Bravo, M.J., Jauch, R., Cojocaru, V., and Schöler, H.R. (2015). Dissecting the role of distinct OCT4-SOX2 heterodimer configurations in pluripotency. Sci. Rep. *5*, 13533.

Theunissen, T.W., and Jaenisch, R. (2014). Molecular control of induced pluripotency. Cell Stem Cell *14*, 720–734.

Thomson, M., Liu, S.J., Zou, L.-N., Smith, Z., Meissner, A., and Ramanathan, S. (2011). Pluripotency factors in embryonic stem cells regulate differentiation into germ layers. Cell *145*, 875–889.

Waddington, C.H. (1957). The Strategy of Genes (New York: Routledge).

Walter, W. (1964). Differential and Integral Inequalities (Berlin: Springer).

Wang, J., Levasseur, D.N., and Orkin, S.H. (2008). Requirement of Nanog dimerization for stem cell self-renewal and pluripotency. Proc. Natl. Acad. Sci. USA *105*, 6326–6331.

Wang, J., Zhang, K., Xu, L., and Wang, E. (2011). Quantifying the Waddington landscape and biological paths for development and differentiation. Proc. Natl. Acad. Sci. USA *108*, 8257–8262.

Warlich, E., Kuehle, J., Cantz, T., Brugman, M.H., Maetzig, T., Galla, M., Filipczyk, A.A., Halle, S., Klump, H., Schöler, H.R., et al. (2011). Lentiviral vector design and imaging approaches to visualize the early stages of cellular reprogramming. Mol. Ther. *19*, 782–789.

Xu, J., Du, Y., and Deng, H. (2015). Direct lineage reprogramming: strategies, mechanisms, and applications. Cell Stem Cell *16*, 119–134.

Yates, J.L., and Guan, N. (1991). Epstein-Barr virus-derived plasmids replicate only once per cell cycle and are not amplified after entry into cells. J. Virol. *65*, 483–488.

STAR★METHODS

KEY RESOURCES TABLE

REAGENT or RESOURCE	SOURCE	IDENTIFIER
Software and Algorithms		
MATLAB R2015a	The Mathworks, Inc.	https://www.mathworks.com/downloads/
Mathematica 10	Wolfram Research	https://www.wolfram.com/mathematica/trial/

CONTACT FOR REAGENT AND RESOURCE SHARING

Further information and requests for resources and reagents should be directed to and will be fulfilled by the Lead Contact Domitilla Del Vecchio (ddv@mit.edu).

METHOD DETAILS

Cooperative Network Reprogramming Properties

We consider a system $\sum_u$ in the form $\dot{x} = f(x,u)$ with $x \in X = \mathrm{R}^n_+$ and $u \in U \subset \mathrm{R}^m_+$ a *constant* input vector. Let S be the set of all stable steady states of $\dot{x} = f(x,0)$, which we refer to as system $\sum_0$. Let $S \in \mathrm{S}$ be one of the stable steady states. We let the flow of system $\sum$ starting from x_0 with input u be denoted by $\phi_u(t,x_0)$ and we will write $\phi_0(t,x_0)$ for the flow of system $\sum_0$. Accordingly, we let $\mathrm{R}_u(S)$ denote the region of attraction, or basin of attraction, of a stable steady state S for system $\sum_u$. That is, $x_0 \in \mathrm{R}_u(S)$ implies that $\lim_{t\to\infty} \phi_u(t,x_0) = S$. Also, we assume that for all $x_0 \in X, u \in U$, the omega-limit set $\omega_u(x_0)$ is finite.

Definition 1. We say that system $\sum_u$ is *strongly reprogrammable* to a steady state $S \in \mathrm{S}$ provided there is an input $u \in U$ such that for all $x_0 \in \mathrm{R}^n_+$ the omega-limit set $\omega_u(x_0)$ is such that $\omega_u(x_0) \subset \mathrm{R}_0(S)$.

From this definition, it follows that, starting from any initial condition x_0, after a sufficiently long application of control input $\bar{u}$, upon removal of such an input, that is, upon setting $u = 0$, the trajectory of $\sum_u$ approaches S. Qualitatively, this means that independent of the initial steady state in which system $\sum_u$ is found, we can force the state to transition to the stable steady state S by a sufficiently long presentation and then removal of a suitable input. In this paper, we seek to determine conditions under which system $\sum_u$ is reprogrammable to a steady state $S \in \mathrm{S}$.

In order to proceed, we assume that system $\sum_u$ is a monotone system. There are two reasons for this assumption: first, many of the biological networks for which the reprogramming question is important are monotone; second, monotonicity allows for strong results about when a system is reprogrammable to a steady state given the rich geometrical properties of the system's trajectories.

Definition 2. Let the state space X be equipped with a partial order relation "$\leq$" (Davey and Priestley, 2002). A system $\sum_u$ is *monotone* provided $x_0 \leq x_0 \Rightarrow \phi_u(t,x_0) \leq \phi_u(t,x_0)$ for all $t \geq 0$ and for all $u \in U$.

In the sequel, we consider the partial order established by component-wise ordering. That is, for all $x, y \in X$ we have $x \leq y$ if and only if $x_i \leq y_i$ for all i.

Assumption 1. System $\sum_u$ is monotone with component-wise partial order relation "$\leq$." Additionally, the system is *cooperative*, that is, $\partial f_i(x,u)/\partial x_j \geq 0$ for $i \neq j$ and for all $x \in X, u \in U$.

Note that a cooperative system is necessarily monotone with ordering on the state space established component-wise (Smith, 1995). To keep the exposition of the theory simple, we chose the component-wise ordering. However, the results provided here naturally extend to any arbitrary partial order established according to a cone. Before giving the main results, we first provide some intermediate properties of the geometry of the stable steady states in a monotone dynamical system.

Proposition 1. *Under Assumption 1, the set of stable steady states* S has a maximum and a minimum.

Proof. Let $\bar{x}$ be any element of X such that $\bar{x} \geq S$ for all $S \in \mathrm{S}$ and let us examine $\omega_0(\bar{x})$. Since $\omega_0(\bar{x})$ is bounded and the system is also cooperative, we have by Proposition 2.1 in (Smith, 1995) that $\omega_0(\bar{x})$ is an equilibrium, which in turn is an element of S. Let $y \in \mathrm{S}$ be such an equilibrium. Since $S \leq \bar{x}$ for each element $S \in \mathrm{S}$, it must be by the monotonicity property that $S \leq \omega_0(\bar{x})$, which, in turn, implies that $S \leq y$ for all $S \in \mathrm{S}$. Therefore, $y = \sup(\mathrm{S})$ and since $y \in \mathrm{S}$ we have that $y = \max(\mathrm{S})$. Hence, **S** has a maximum. A similar proof holds for the minimum. ■

Now, we can state the first result. For a matrix M, we write $M \geq 0$ when $M_{ij} \geq 0$ for all i, j.

Theorem 1. *For system* $\sum_u$ assume that $(\partial f(x,u)/\partial u) \geq 0$ for all $x \in X, u \in U$ (positive perturbation) and let Assumption 1 hold. Then, system $\sum_u$ is not strongly reprogrammable to any $S \neq \max(\mathrm{S})$.

Proof. First, we show that for all $u > 0$ system $\dot{x} = f(x,u)$ always admits a stable steady state $\bar{x}$ such that $\bar{x} \geq S$ for all $S \in \mathrm{S}$. Using a similar approach as used in Nikolaev and Sontag (2016), we can consider the extended system

$$\dot{x} = f(x,u),\ \dot{u} = 0$$

which is also monotone with order on U established component-wise. Consider two trajectories starting from the two initial conditions $(x_0, u_0) \leq (x_0, u_0)$ given by $x_0 = x_{0'} = \max(S)$ and $u_0 = 0$, $u_{0'} > 0$. Since $(x_0, 0)$ is a steady state of the above system, by the monotonicity property we have that $x_0 \leq \phi_{u_{0'}}(t, x_{0'})$ for all t. Hence we have that in system $\dot{x} = f(x, u_{0'})$, $\omega_{u_{0'}}(\max(S))$ is greater than $\max(S)$ itself. In turn, consider $\dot{x} = f(x, 0)$ and an initial condition $z \geq \max(S)$. By the monotonicity property, we have that $\omega_0(z) \geq \max(S)$. Since there is no equilibrium of $\dot{x} = f(x, 0)$ in the cone $\{x \mid x \geq \max(S)\}$ and by Proposition 2.1 in (Smith, 1995) $\omega_0(\overline{x})$ is an equilibrium, we must have that $\omega_0(z) = \max(S)$. We conclude that for $\sum_u$ with $u > 0$ there is x_0 such that $\omega_u(x_0) \in R_0(\max(S))$, therefore $\sum_u$ cannot be reprogrammed to any of the steady states in S that are different from the maximal one.

This result indicates that in a monotone (cooperative) system with only positive stimuli, it is not possible to strongly reprogram the system to any of the stable states that are not maximal. ■

Lemma 1. *Consider system* $\sum_u$ satisfying Assumption 1 with $f_i(x, u_i) = H_i(x) + u_i - \gamma_i x_i$, $0 \leq H_i(x) \leq H_{iM}$ for all $x \in X$, and $\varepsilon < \varepsilon^*$. Then, $\lim_{t \to \infty} x_i(t) \geq \max_{S \in S}(S)$ independent of the initial condition.

Proof. Consider the system with $u = 0$ given by $\dot{x}_i = f_i(x, 0) = H_i(x) - \gamma_i x_i$ for all $i \in \{1, \cdots, n\}$. Here, we can view $H_i(x)$ as a bounded disturbance and can therefore apply the robustness result from contraction theory (Del Vecchio and Slotine, 2013) to obtain that $x_i(t) \leq Ae^{-\gamma_i t} + (H_{iM}/\gamma_t)$ for some positive A depending on the initial condition. Letting $\overline{x}_i := \lim_{t \to \infty} x_i(t)$, we have that, $\overline{x}_i \leq (H_{iM}/\gamma_i)$. Since $\overline{x}_i$ is an unspecified equilibrium point of $\sum_0$, we have, in particular, that $\max(S_i) \leq (H_{iM}/\gamma_i)$.

Now, consider the pair of systems:

$$\dot{z}_i = u_i - \gamma_i z_i, \quad \dot{\tilde{x}}_i = H_i(\tilde{x}) - \gamma_i \tilde{x}_i + u_i,$$

in which we can view the first system as a nominal system and the second system as its perturbed version with disturbance $H_i(\tilde{x})$, which is globally bounded by H_{iM}. Hence, we can apply again the robustness result from contraction theory to obtain

$$\lim_{t \to \infty} \left| \tilde{x}(t) - \frac{u_i}{\gamma_i} \right| \leq \frac{H_{iM}}{\gamma_i}$$

Letting $\varepsilon := H_{iM}/u_i$ and re-arranging the terms, we obtain that $\lim_{t \to \infty} \tilde{x}(t) - (u_i/\gamma_i)(1 - \varepsilon)$. Since for $u_i \geq 2H_{iM}$, we have that $(u_i/\gamma_i)(1 - \varepsilon) \geq (H_{iM}/\gamma_i)$, we also have that $\lim_{t \to \infty} \tilde{x}(t) \geq \max(S_i)$. ■

Lemma 2. *Assume that system* $\sum_u$ satisfies Assumption 1 and that it is in the following form: $\dot{x}_i = f_i(x, u_i) = H_i(x) - \gamma_i x + u_i$ with $u_i \in \mathbb{R}_+$ and $0 \leq H_i(x) \leq H_{iM}$ for all $x \in X$. Then, if $u_i \geq 2H_{iM}$ for all $i \in \{1, \ldots, n\}$, then $\omega_0(x_0) \geq \max(S)$ for all $x_0 \in X$.

Proof. By using Lemma 1, for system $\sum_u$ with $u_i \geq 2H_{iM}$ for all i we have that $\lim_{t \to \infty} x_i(t) \geq \max_{S \in S}(S_i)$ for all i independent of the initial condition. Since this is true for any initial condition $x(0) = x_0$, we have that $\omega_u(x_0) \geq \max(S)$ for all $x_0 \in X$. ■

Theorem 2. *Assume that system* $\sum_u$ satisfies Assumption 1 and that it is in the following form: $\dot{x}_i = f_i(x, u_i) = H_i(x) - \gamma_i x + u_i$ with $u_i \in R_+$ and $0 \leq H_i(x) \leq H_{iM}$ for all $x \in X$. Then, system $\sum_u$ is strongly reprogrammable to S if and only if $S = \max(S)$. In particular, a sufficiently large input will reprogram $\sum_u$ to $\max(S)$.

Proof. It follows from Theorem 1 and Lemma 2. ■

Strong reprogrammability of the system to S requires that *all* possible initial conditions can be steered to the region of attraction of S for some constant input u. The system is not strongly reprogrammable to any intermediate state because initial conditions that are greater than the maximal element of S will be kept in the region of attraction of this maximal element independent of the input chosen. We therefore investigate whether a weaker reprogrammability to an intermediate state S holds, in which *some* initial condition not in the region of attraction of S can be steered to the region of attraction of S with constant input perturbation. We thus give the following definition.

Definition 3. We say that system $\sum_u$ is *weakly reprogrammable* from steady state $\overline{S} \in S$ to a steady state $S \in S$ with $\overline{S} \neq S$ provided there is an input $u \in U$ such that the omega-limit set $\omega_u(\overline{S})$ is such that $\omega_u(\overline{S}) \subset R_0(S)$.

The following result shows that if $\overline{S} > S$, then the system cannot be weakly reprogrammed from $\overline{S}$ to S.

Proposition 2. *Let* $S, \overline{S} \in S$ and let $S < \overline{S}$. Then, system $\sum_u$ is not weakly reprogrammable from $\overline{S}$ to S.

Proof. Systems $\sum_u$ and $\sum_0$ are both monotone cooperative systems with $f(x, 0) \leq f(x, u)$. It follows from Theorem VI (page 94 of Walter [1964]) that $\phi_0(t, \overline{S}) \leq \phi_u(t, \overline{S})$ for all t. Also, we have that $\phi_0(t, \overline{S}) = \overline{S}$. Therefore, we have that $p := \omega_u(\overline{S}) \geq \overline{S}$. Since $p \geq \overline{S}$, we have that $\phi_0(t, p) \geq \overline{S}$ for all t. This implies that $\omega_0(p) \geq \overline{S}$, and therefore that p is not in the region of attraction of S since $S < \overline{S}$.

The last result shows that if $\overline{S} < S$ but the input is either too large or too small, the trajectory of $\sum_u$ will not approach the region of attraction of S.

Proposition 3. *Let* $S, \overline{S} \in S$ and let $\overline{S} < S$. There are inputs u_1 *and* u_2 *such that if* $u \leq u_1$ or $u \leq u_2$, then $\sum_u$ is not weakly reprogrammable from $\overline{S}$ to S.

Proof. Consider $\sum_u$ with u small. Since $\overline{S}$ is a stable equilibrium for $\sum_0$, it follows that $\partial f(x, u)/\partial x \mid_{\overline{S}, 0}$ is Hurwitz and hence non-singular. Since it is a continuous function of u and x, it follows from the implicit function theorem that there is an open ball $B \subset U$ about $u = 0$ such that $\overline{x}(u)$ is a locally unique solution to $f(x, u) = 0$ for $u \in B$; furthermore $\overline{x}(u)$ is a continuous function of u. Therefore, for small u, we will have that $\overline{x}(u)$ is close to $\overline{S}$. We can thus pick u small enough such that $\overline{x}(u)$ is in the region of attraction of $\overline{S}$. Also, we have that $\overline{x}(u) \geq \overline{S}$ for the monotonicity property of the systems $\sum_0$ and $\sum_u$. Therefore a trajectory $\phi_u(t, \overline{S})$ will asymptotically reach a point p that is always smaller than $x(u)$ and hence in the region of attraction of $\overline{S}$. Therefore, there is an input $u_1 > 0$ sufficiently small such that if $u \leq u_1$ the system is not reprogrammed from $\overline{S}$ to S.

Consider $\sum_u$ with u large. The fact that there is u_2 sufficiently large such that if $u \geq u_2$ the system is not reprogrammed from $\overline{S}$ to S follows from Lemma 2.

This result implies that system $\sum_u$ with $u \leq u_1$ or $u \leq u_2$ is not weakly reprogrammable to any intermediate state $S \in$ S from the minimum of S. In other words, the system *may* be reprogrammed to the intermediate steady state S from the minimum one only if u takes values in an intermediate range $[u_1, u_2]$, which, however, may be empty since we may have $u_2 < u_1$.

Two-node example.

The parameters corresponding to the nullclines of Figure 2B are given by: $a_1 = 0.276$, $b_1 = 1.38$, $c_1 = 0.897$, $a_2 = 0.00828$, $b_2 = 0.0828$, $c_2 = 0.092$, $d = 1$, $\gamma_1 = 0.138$, and $\gamma_2 = 0.046$. The values of u_1 are: 0.0041, 0.017, and 0.0025. The values of u_2 are: 0.00085, 0.00027, and 0.0041.

Figure S1 illustrates a case where overexpression values exist to reprogram the network from S_1 to S_0 Only initial conditions belonging to the green shaded area in Figure S1 lead to trajectories approaching $S_{0'}$, while any other initial condition will lead to trajectories approaching the top-right steady state. After these trajectories have reached their corresponding steady states, removal of the stimulus (Figure S1, right-side) leads the trajectories initiated in the green area to approach S_0, while the others approach S_2.

Type 1 Interactions and Reprogramming Properties

In this section, we demonstrate that the addition of a Type 1 interaction to a monotone cooperative network keeps the extended network monotone and cooperative in possibly new coordinates for the variables of the added interactions.

Specifically, let $y \in \mathrm{R}^m$ represent the vector of concentrations of additional species added to the original network. The full system is now given by

$$\dot{y} = g(y, x), \quad \dot{x} = \tilde{f}(x, y, u), \quad \text{with } \tilde{f}(x, 0, u) = f(x, u).$$

Consider any two nodes x_j and x_k and consider a path $x_j \to y_{j_1} \to \ldots \to y_{j_p} \to x_k$ such that

$$\frac{\partial g_{j_1}}{\partial x_j}, \frac{\partial g_{j_2}}{\partial x_{j_1}}, \ldots \frac{\partial g_{j_p}}{\partial x_{j_{p-1}}}, \frac{\partial \tilde{f}_k}{\partial y_{j_p}}$$

are all not identically zero. Consider the restricted system in which the y dynamics take as "input" only x_j through only the interaction $x_j \to y_{j_1}$ and the x dynamics take as input only y_{j_p} through only the interaction $y_{j_p} \to x_k$. The dynamics of this system are given by:

$$\dot{y}_{-j_i} = g_{-j_i}(y, 0), \quad \dot{y}_{j_i} = g_{j_i}(y, (0, \ldots, x_j, \ldots 0)), \quad \dot{x}_{-k} = \tilde{f}_{-k}(x, 0, u), \quad \dot{x}_k = \tilde{f}_k\left(x, \left(0, \ldots, y_{j_p}, \ldots 0\right), u\right), \tag{Equation S1}$$

in which for a vector v, we have denoted by v_k its kth component and by v_{-k} the vector v with the kth component removed. In the sequel, for a vector v and a diagonal matrix with entries the vector's coordinates $M = diag(v)$ we denote by M_{-i} the $n-1 \times n-1$ diagonal matrix given by diag(m_{-1}).

We now consider interactions that do not change the monotone cooperative structure of the system. To this end, we make the following simplifying assumption.

Assumption 2. For system (SI-1), we assume that each y_{j_i} in the path $x_j \to y_{j_1} \to \ldots \to y_{j_p} \to x_k$ has only one parent and only one child, that is, the path is *simple*.

$$\dot{y}_{j_1} = g_{j_1}\left(y_{j_1}, (0, \ldots, x_j, \ldots, 0)\right), \ldots, \dot{y}_{j_{i+1}} = g_{j_{i+1}}\left(y_{j_i}, 0\right), i \leq p-1, \dot{x}_k = \tilde{f}_k\left(x, \left(0, \ldots, y_{i_p}, \ldots 0\right)\right), \tag{Equation S2}$$

and

$$\dot{y}_- = g_-(y_-, 0),$$

in which y_- is the vector y with the components $y_{j_1}, \ldots, y_{j_p}$ removed. We now give the following definition of a Type 1 interaction. Let Λ be a diagonal matrix with diagonal entries $\lambda_i \in \{-1, 1\}$. We then give the following definition.

Definition 4. The simple path $x_j \to y_{j_1} \to \ldots \to y_{j_p} \to x_k$ is a *Type 1 interaction* provided there is a Λ such that system (Equations S1 and S2) in the new coordinates $\overline{y} = \Lambda y$ is a cooperative monotone system.

This definition implies that a Type 1 interaction extends the original x system to the larger system (given by Equation S2) that in the new coordinates $\overline{y} = \Lambda y$ becomes

$$\dot{\overline{y}}_{j_1} = \lambda_{j_1} g_{j_1}\left(\lambda_{j_1}\overline{y}_{j_1}, (0, \ldots, x_j, \ldots, 0)\right), \ldots \dot{\overline{y}}_{j_{i+1}} = \lambda_{j_{i+1}} g_{j_{i+1}}\left(\lambda_{j_i}\overline{y}_{j_1}, 0\right), i \leq p-1, \dot{x}_k = \tilde{f}_k\left(x, \left(0, \ldots \lambda_{j_p}\overline{y}_{j_p}, \ldots 0\right)\right), \tag{Equation S3}$$

which is still monotone and cooperative with the component-wise order $x \leq x' \Leftrightarrow x_i \leq x_{i'} \ \forall i$ according to which the isolated x system is also cooperative. It follows that this system is also not strongly reprogrammable to the intermediate state PL and may be weakly reprogrammable to it from a lower steady state, such as TR, for some range of inputs.

With these premises, we can provide a check for when a simple path is a Type 1 interaction.

Proposition 4. *Consider system (SI-2). If the condition*

$$\frac{\partial g_{j_1}}{\partial x_j} \cdot \frac{\partial g_{j_2}}{\partial y_{j_1}} \cdot \frac{\partial g_{j_p}}{\partial y_{j_{p-1}}} \cdot \frac{\partial \tilde{f}_k}{\partial y_{j_p}} \geq 0 \tag{Equation S4}$$

is satisfied, then the path is a Type 1 interaction.

Proof. It is sufficient to prove that there are $\lambda_{j_1},\ldots,\lambda_{j_p}$ that each take value in $\{-1,1\}$ such that

$$\frac{\partial g_{j_1}}{\partial x_j}\lambda_{j_1}\geq 0,\quad \frac{\partial g_{j_2}}{\partial y_{j_1}}\lambda_{j_1}\lambda_{j_2}\geq 0,\ldots,\frac{\partial g_{j_p}}{\partial y_{j_{p-1}}}\lambda_{j_{p-1}}\lambda_{j_p}\geq 0,\quad \text{and}\quad \frac{\partial \tilde{f}_k}{\partial y_{j_p}}\lambda_{j_p}\geq 0.$$

This, in turn is the case if and only if we have

$$\lambda_{j_1}=\text{sign}\left(\frac{\partial g_{j_1}}{\partial x_j}\right),\quad \lambda_{j_2}=\text{sign}\left(\frac{\partial g_{j_1}}{\partial x_j}\frac{\partial g_{j_2}}{\partial y_{j_1}}\right),\ldots,\lambda_{j_p}=\text{sign}\left(\frac{\partial g_{j_1}}{\partial x_j}\frac{\partial g_{j_2}}{\partial y_{j_1}}\bullet\ldots\bullet\frac{\partial g_{j_p}}{\partial y_{j_{p-1}}}\right),$$

and

$$\lambda_{j_p}=\text{sign}\left(\frac{\partial \tilde{f}_k}{\partial y_{j_p}}\right).$$

This set of equations has a solution if and only if

$$\text{sign}\left(\frac{\partial \tilde{f}_k}{\partial y_{j_p}}\right)=\text{sign}\left(\frac{\partial g_{j_1}}{\partial x_j}\frac{\partial g_{j_2}}{\partial y_{j_1}}\bullet\ldots\bullet\frac{\partial g_{j_p}}{\partial y_{j_{p-1}}}\right),$$

which is, in turn true by the assumed condition (Equation S4).

We will refer to a simple path where condition (Equation S4) is satisfied as a *positive interaction*. We will refer to a simple path where condition (Equation S4) is not satisfied as a *negative interaction*. In this case, by the same argument as those in the above proof, the system (Equation S2) does not admit a coordinate change Λ such that the system in the new coordinates is monotone and cooperative. If the path is not simple, the left-hand side of (Equation S4) loses meaning and we will refer to these paths as *undetermined interactions*. We will refer to negative or undetermined interactions as Type 2 interactions.

Type 2 Interactions and Reprogramming Properties

Given a monotone system Σ_u of the cooperative type

$$\Sigma_u:\ \dot{x}=f(x,u),f_i(x,u)=H_i(x)-\gamma_i+u_i,i\in\{1,\ldots,n\}$$

as before with a set of partially ordered stable steady states for Σ_u given by $S_u=\{S_u^1,\ldots,S_u^m\}$, in which we assume without loss of generality that S_u^1 is the minimum and S_u^m is the maximum. We now consider an undetermined perturbation to this dynamics as follows:

$$\Sigma_u^\varepsilon:\ \dot{x}=f(x,u)+Ed(x),\quad \varepsilon>0,\quad \|d(x)\|\leq d_M,\forall\ x$$

in which $d(x)$ is a bounded perturbation that captures the effect of unmodeled interactions. Here, we assume that all functions are smooth. We also assume that the omega-limit set of any initial condition of Σ_u^ε is a steady state.

Here, we seek to demonstrate that if ε is sufficiently small, then we still have the reprogramming properties of Σ_u. Namely, the system is not strongly reprogrammable to any stable steady state different from the continuation of S_0^m with $\varepsilon>0$ small. Furthermore, the system is not weakly reprogrammable from the continuation of S_0^1 to any steady state that is the continuation of an intermediate steady state of Σ_0 with inputs that are either too large or too small.

The following theorem shows that for ε small enough, the stable steady states of Σ_u^ε lie within an ε ball around the stable steady states of Σ_u.

Lemma 3. *There is* $\varepsilon^*>0$, smooth functions $\gamma_u^1(\varepsilon),\ldots,\gamma_u^m(\varepsilon)$, and $c>0$ such that for $\varepsilon<\varepsilon^*$ we have

(i) $\|\gamma_u^i(\varepsilon)-S_u^i\|\leq c\varepsilon$;
(ii) $x=\gamma_u^i(\varepsilon)$ *is a stable steady state for* Σ_u^ε *for any i.*

Proof. Let us call $F(x,\varepsilon):=f(x,u)+\varepsilon d(x)$ such that $F(x,0)=f(x,u)$. Since $F(\bullet,\bullet)$ is a smooth function of its arguments and $(\partial F/\partial x)\,|_{(S_u^i,0)}$ is Hurwitz (because S_u^i is a locally asymptotically stable equilibrium point), by the implicit function theorem there is $\varepsilon_1^*>0$ and a locally unique smooth function $\gamma_u^i(\varepsilon)$, such that $F(\gamma_u^i(\varepsilon),\varepsilon)=0$ for all $\varepsilon<\varepsilon_1^*$. Also, $(d\gamma_u^i/d\varepsilon)=(\partial F/\partial x)^{-1}(\partial F/\partial\varepsilon)$. Let c be the supremum over $\varepsilon\in[0,\bar{\varepsilon}]$ with $\bar{\varepsilon}<\varepsilon_1^*$ of $\|(d\gamma_u^i/d\varepsilon)\|$, then $\|\gamma_u^i(\varepsilon)-\gamma_u^i(0)\|\leq c\bullet\varepsilon$ which leads to (i). The fact that $x=\gamma_u^i(\varepsilon)$ is a steady state of Σ_u^ε follows from the fact that $F(\gamma_u^i(\varepsilon),\varepsilon)=0$ for all $\varepsilon<\varepsilon^*$. The fact that it is stable follows from the following argument. Define the matrix $g(\varepsilon)=(\partial F/\partial x)\,|_{(\gamma_u^i(\varepsilon),\varepsilon)}$. By the problem definition, we have that the eigenvalues of $g(0)$ all have strictly negative real parts. Since g is a smooth function of ε and the roots of the characteristic polynomial of g depend continuously on its coefficients, there is ε' such that $g(\varepsilon)$ has eigenvalues with strictly negative real part for all $\varepsilon<\varepsilon'$. Therefore, (ii) follows with $\varepsilon^*=\min\{\varepsilon',\varepsilon_1^*\}$. ■

In the sequel, we assume that ε is small enough such that this Lemma holds and also such that the balls $B_{c\varepsilon}(S_u^i)$ for $i\in\{1,\ldots,m\}$ are disjoint. Such an ε exists because the steady states in S_u are isolated.

Lemma 4. *Let* $x(t,x_o)$ denote the trajectory of $\Sigma_u^\varepsilon:\ \dot{x}=f(x,u)+\varepsilon d(x)$, let $w(t,w_o)$ denote the trajectory of $\Sigma_u^M:\ \dot{w}=f(w,u)+\varepsilon d_M$, and let $v(t,v_o)$ denote the trajectory of $\tilde{\Sigma}_u:\ \dot{x}=f(x,u)-\varepsilon d_M$ starting from initial conditions $v_o\le x_o\le w_o$. Then, we have that $v(t,v_o)\le x(t,x_o)\le w(t,w_o)$ for all $t\ge 0$.

Proof. The result follows directly from Theorem VI (page 94 of Walter [1964]) applied to the pairs $\dot{x},f(x,u)$ and $\dot{x},f(x,u)-\varepsilon d_M$, in which the vector fields $f(x,u)$ and $f(x,u)-\varepsilon d_M$ are each quasi-monotone according to the definition in Walter (1964). ■

This result says that the trajectories of Σ_u^ε are always comprised between those of $\tilde{\Sigma}_u$ and those of Σ_u^M.

Consider the set of stable steady states of $\tilde{\Sigma}_u$. For ε sufficiently small, the same arguments as those in Lemma 3 applied to Σ_u^ε apply and therefore this set will be given by $\tilde{S}$: $\{\tilde{S}_u^1,\dots,\tilde{S}_u^m\}$, in which $\tilde{S}_u^i$ lies within a ball with radius proportional to ε centered at S_u^i. Also, since $\tilde{\Sigma}_u$ is monotone and cooperative, we have that the set of stable steady states has a maximum and a minimum. Without loss of generality, let $\tilde{S}_u^m$ be the maximum and $\tilde{S}_u^1$ be the minimum. Then, we have the following Lemma.

Lemma 5. *Let* x_o be the initial condition of Σ_u^ε. If $x_o\ge\tilde{S}_u^m$, then $\omega_u^\varepsilon(x_o)\ge\tilde{S}_u^m$.

Proof. By Lemma 4, we have that if $v_o=x_o$ then $v(t,v_o)\le x(t,x_o)$ for all $t\ge 0$. This inequality continues to be true asymptotically, and therefore, we must also have that $\omega_u^\varepsilon(x_o)\ge\lim_{t\to\infty}v(t,v_o)$. In turn, since system $\tilde{\Sigma}_u$ is monotone and cooperative and $v_o\ge\tilde{S}_u^m$, then we must have that $\lim_{t\to\infty}v(t,v_o)=\tilde{S}_u^m$, leading to the desired result. ■

This lemma implies that Σ_u^ε for any $u>0$ has a steady state that is greater than $\tilde{S}_0^m$ (since $\tilde{S}_u^m$ is greater than any of the stable steady states $\tilde{S}_0^i$ by the monotonicity property along with positive perturbation).

Theorem 3. *System* Σ_u^ε is not strongly reprogrammable to any stable steady state of Σ_0^ε different from $\gamma_0^m(\varepsilon)$.

Proof. By Lemma 5, any $u>0$ for Σ_u^ε will result for $x_o\ge\tilde{S}_u^m$ in a stable steady state that is greater than $\tilde{S}_u^m$ and hence of $\tilde{S}_0^m$ since $\tilde{S}_u^m$ is greater than any of the stable steady states $\tilde{S}_0^i$ by the monotonicity property along with positive perturbation. A trajectory $x(t,x_o)$ of Σ_0^ε that starts with $x_o\ge\tilde{S}_0^m$ will be such that (by Lemma 5) $\omega_u^\varepsilon(x_o)\ge\tilde{S}_0^m$. It will therefore converge to a stable steady state of Σ_0^ε that is greater than or equal to $\tilde{S}_0^m$. By Lemma 3, the only such steady state is $\gamma_0^m(\varepsilon)$. Since there are always initial conditions that give rise to trajectories approaching the region of attraction of $\gamma_0^m(\varepsilon)$, it follows that the system is not strongly reprogrammable to any other stable steady state. ■

Theorem 4. *There are* $u_1,u_2>0$ such that if $u\le u_1$ or $u\ge u_2$ then Σ_u^ε is not weakly reprogrammable from $\gamma_0^1(\varepsilon)$ to any $\gamma_0^i(\varepsilon)$ for $i\ne m$.

Proof. From Lemma 2 with $H_i(x)$ re-defined as $H_i(x)+\varepsilon d_i(x)$, we have that for all x_o, the trajectory of Σ_u^ε with $u_i\ge 2H_{iM}$ for all i will result into $\omega_u(x_o)\ge\tilde{S}_0^m$. As a consequence, $\omega_u(x_o)\in R_0(\gamma_0^m(\varepsilon))$ for all x_o and in particular for $x_o=\gamma_0^1(\varepsilon)$. Reversely, if u is too small, by continuity arguments $x_o=\gamma_0^1(\varepsilon)$ will approach a steady state that still lies in the region of attraction of $\gamma_0^1(\varepsilon)$. ■

Properties of High-Gain Negative Feedback

Consider the ODE (3):

$$\dot{x}_i=H_i(x)-\gamma_i x_i+G_i\left(x_i^*-x_i\right),$$

in which $|H_i(x)|\le H_M$ for all x. Now consider the error $e=x_i-x_i^*$ and re-write the above dynamics in error coordinates:

$$\dot{e}=H_i(x)-\gamma_i x_i^*-e(G_i+\gamma_i).$$

In this system $H_i(x)-\gamma_i x_i^*$ can be viewed as a bounded disturbance such that $\left|H_i(x)-\gamma_i x_i^*\right|\le H_M+\gamma_i x_i^*$. Since this system is contracting with contraction rate $G_i+\gamma_i$, we can use the robustness result from contraction theory (Del Vecchio and Slotine, 2013) to conclude that

$$\left|x_i(t)-x_i^*\right|\le C_1e^{-G_i^t}+\frac{H_m+\gamma_i x_i^*}{G_i+\gamma_i},$$

leading to a faster convergence rate as G_i increases and ultimately leading to

$$\text{limsup}_{t\to\infty}\left|x_i(t)-x_i^*\right|\le\frac{H_m+\gamma_i x_i^*}{G_i+\gamma_i}.$$

Synthetic Feedback Controller Circuit

Consider the ODE model in Equation 8. Exploiting the fact that the association and dissociation reactions in an enzymatic reaction are much faster than the catalytic reaction (Del Vecchio and Murray, 2014), we can re-write the system in the slow variables $\bar{s}_i=s_i+c_i$ and $\bar{m}_i=m_i+c_i$ and approximate the complex c_i to its quasi-steady state

$$c_i=\bar{s}_i\frac{m_i/K_m}{1+m_i/K_m},\quad K_m=(d_i+k_i)/a_i,$$

in which K_m is the Michaelis-Menten constant of the mRNA/sRNA reaction. This leads to the new set of ODEs

$$\dot{\bar{s}}_i=Dh_{i,2}(I_{i,2})-\beta_i\bar{s}_i,\quad\dot{\bar{m}}_i=\overline{H}_i(x)-\delta_i m_i-k_i\bar{s}_i\frac{m_i/K_m}{1+m_i/K_m}+Dh_{i,1}(I_{i,1}),\quad\dot{x}_i=\kappa_i m_i-\gamma_i x_i,$$

in which, we have made the approximation $\beta_i=k_i$, since dilution is typically much slower than catalytic reactions (Del Vecchio and Murray, 2014). From Haley and Zamore (2004), it is known that $m_i\ll K_m$ for physiologically relevant values of mRNA concentration.

Also, with the synthetic genetic controller, we expect to keep the mRNA concentration within physiologically relevant values through the entire control operation since overexpression is applied concurrently with enhanced mRNA degradation. As a consequence, we can simplify the above system to

$$\dot{\bar{s}}_i = Dh_{i,2}(I_{i,2}) - \beta_i \bar{s}_i, \quad \dot{\bar{m}}_i = \overline{H}_i(x) - \delta_i m_i - \frac{k_i \bar{s}_i}{K_m} m_i + Dh_{i,1}(I_{i,1}), \quad \dot{x}_i = \kappa_i m_i - \gamma_i x_i, \qquad \text{(Equation S5)}$$

in which, assuming that $\bar{s}_i$ has already reached its steady state given by $D\alpha_i/\beta_i$, we can set

$$G_i = \frac{k_i}{K_m}\frac{D\alpha_i}{\beta_i}, \quad m_i^* = \frac{h_{i,1}(I_{i,1})}{\alpha_i}\frac{K_m\beta_i}{k_i}. \qquad \text{(Equation S6)}$$

Therefore, the above system finally becomes

$$\dot{\bar{m}}_i = \overline{H}_i(x) - \delta_i m_i + G_i\left(m_i^* - m_i\right), \quad \dot{x}_i = \kappa_i m_i - \gamma_i x_i,$$

which has the same form as the system in Equation 7 in the main text, in which a one-step reaction was assumed. This leads to the same conclusion: we have a globally asymptotically stable system with unique equilibrium point given by

$$m_i^* = \frac{h_{i,1}(I_{i,1})}{\alpha_i}\frac{K_m\beta_i}{k_i}, \quad x_i^* = \frac{k_i m_i^*}{\gamma_i}$$

for G_i sufficiently large.

Parameter feasibility analysis and numerical simulations.

We perform a feasibility study to determine what DNA concentrations D need to be used in order to ensure sufficiently large G_i, that is, $G_i \gg \delta_i$ and $G_i m_i \gg \overline{H}_i(x)$, in which the expression of G_i is given in Equation S6. This is the only requirement for the control design to stabilize the concentration x_i to the prescribed value x_i^*. From the half-lives of TFs' mRNA, such as Nanog and Oct4, we can estimate $\delta_i \in [0.09, 0.17]$ hr^{-1} (Sharova et al., 2009). Also, from the in vitro study of Haley and Zamore (2004), we know that for completely complementary siRNA we can obtain $k_i \approx 61$ hr^{-1}. We can estimate the maximal promoter induction, $\alpha_i = h_{i,2}(I_{i,2})$, using the typical transcription initiation rate in mammalian cells. The initiation rate for transcription in mammalian cells was estimated to be about 0.0216 s^{-1}, but only 8.6% of RNAP that arrive at the initiation step are estimated to result in an mRNA molecule product (Darzacq et al., 2007). Therefore, we take an effective transcription initiation rate of 0.0018 s^{-1}, or equivalently $\alpha_i = 6.7$ hr^{-1} for a maximally induced promoter. Considering that dilution rate is about $\beta_i \approx 0.05$ hr^{-1}, corresponding to a doubling time of 20 hr (Milo et al., 2010), in the worst case scenario when $K_m = 1$ nM the gain is given by

$$G_i \approx D\frac{61 \cdot 6.7}{1 \cdot 0.05} = 8,174D.$$

Requesting that $G_i \geq 10\delta_i$ with $\delta_i = 0.17$ hr $-\delta_i m_i$ then leads to

$$D \geq 0.0002 \text{ nM} \leftrightarrow \text{D copy number} \geq 1.$$

Similarly, we can find the copy number of D needed to make $G_i m_i \gg \overline{H}_i(x)$. To this end, we estimate the maximal value of $\overline{H}_i(x)$ from the maximal rate of transcription used above, $\alpha_i = 6.7$ hr^{-1}, and from the fact that this should be multiplied by the concentration of DNA. Since the endogenous system is on the chromosome, which is in one copy, it has a concentration of $0.4 \cdot 10^{-3}$ nM (Milo et al., 2010), so that we estimate an upper bound of $\overline{H}_i(x)$ given by $\bar{s}_i(m_i/K_m)/(1 + p_i/K_d)$. Given that mRNA levels of proteins in mammalian cells have a median of about 17 molecules per cell (Schwanhäusser et al., 2011), we can use for our estimates $m_i^* \approx$ 0.02 nM. Since from the above calculations we have $G_i \approx 8,174D$, it is therefore sufficient to have

$$8,174D \cdot 0.006 \geq 10 \cdot 2.68 \cdot 10^{-3} \rightarrow D \geq 5.4 \cdot 10^{-4} \text{ nM}$$

which is guaranteed if D is at least in one copy. Based on these calculations, with a few copies of the synthetic genetic circuit, we will be able to realize a sufficiently high gain G_i, which leads to stabilizing the concentration x_i to the prescribed value x_i^*.

Provided $G_i \gg \delta_i$, $G_i m_i^* \gg \overline{H}_i(x)$, and $m_i \ll K_M$, the specific concentrations of the species are not relevant to the functioning of the synthetic genetic controller circuit. Therefore, we considered arbitrary units (AU) of concentration in the simulations. Units of time, instead, were considered in hours in order to provide information about the speed at which the synthetic genetic controller can steer the TF concentrations to their prescribed values. The simulation parameter values are in Table S1.

Figure S2A shows the effect of decreasing the gain G_i (by decreasing the circuit DNA D copy number) on the controller performance. As D is decreased, the steady state reached by x_1 and x_2 starts deviating from the prescribed concentrations x_1^* and x_2^* and the time to reach steady state substantially increases.

Feedback Controller Shutdown

When the controller is shut down, that is, when $I_{i,1}$ and $I_{i,2}$ for $i \in \{1,2\}$ are set back to zero, s_i(t) does not reach zero immediately. Before s_i(t) reaches zero it can, in principle, push the state of the system out of the region of attraction of S_0 and hence it is desirable to speed up its removal. In order to resolve this potential problem, upon setting $I_{i,1} = 0$ and $I_{i,2} = 0$ for $i \in \{1,2\}$, we also induce mRNA sponge p_i

(through inducer $I_{i,3}$) for $i \in \{1,2\}$ that quickly sequesters the siRNA from its targets m_i^s and m_i^e (Jens and Rajewsky, 2015; Ebert et al., 2007). We model the sponging effect by sequestration wherein the sponge reversibly binds with its siRNA target. Specifically, we have:

$$p_i + s_i \underset{\tilde{d}_i}{\overset{\tilde{a}_i}{\rightleftharpoons}} c_{p_i}, \quad K_d = \frac{\tilde{d}_i}{\tilde{a}_i}, \quad c_{p_i} \xrightarrow{\beta_i} \varnothing.$$

Assuming a decay rate $\tilde{\delta}_i$ for the sponge p_i, we have that system (Equation 8) after setting the inducers to zero, that is $I_{i,1} = I_{i,2} = 0$, and inducing the sponges, transforms into

$$\begin{aligned} &\dot{\bar{s}}_i = -\beta_i \bar{s}_i, s_i(0) = \frac{D h_{i,2}(I_{i,2})}{\beta_i}, && \dot{c}_i = a_i m_i s_i - (d_i + k_1) c_i - \beta_i c_i \\ &\dot{m}_i = \bar{H}_i(x) - \delta_i m_i - a_i m_i s_i + d_i c_i, && \dot{x}_i = \kappa_i m_i - \gamma_i x_i, \\ &\dot{p}_i = \bar{D} h_{i,3}(I_{i,3}) - \tilde{\delta}_i p_i - \tilde{a}_i p_i s_i + \tilde{d}_i c_{p_i}, && \dot{c}_{p_i} = \tilde{a}_i p_i s_i - \tilde{d}_i c_{p_i} - \beta_i c_{p_i}, \quad s_i = \bar{s}_i - c_i - c_{p_i}, \end{aligned} \tag{Equation S7}$$

in which $\bar{D}$ is the concentration of the DNA where the sponge is encoded and $h_{i,3}(\cdot)$ is the inducer regulation function. This set of ODEs models the dynamics of the system after the controller is shut down. For this system, we can mathematically determine conditions on key parameters, such as the DNA copy number $\bar{D}$, such that the speed of siRNA removal is sufficiently fast to ensure that $(m(t), x(t))$ will remain in the region of attraction of S_0 during the shutdown process, leading $(m(t), x(t))$, and thus $(m^e(t), x^e(t))$, to converge to S_0.

To this end, we reduce this system to the slow variable dynamics by setting the complex dynamics to the quasi-steady state and re-writing the system in the slow variables $\bar{m}_i = m_i + c_i$ and $\bar{p}_i = p_i + c_{p_i}$:

$$\begin{aligned} &\dot{\bar{s}}_i = -\beta_i \bar{s}_i, && \dot{c}_i = \bar{s}_i \frac{m_i/K_m}{1 + p_i/K_d}, c_{p_i} = \bar{s}_i \frac{p_i/K_d}{1 + p_i/K_d} \\ &\dot{\bar{m}}_i = \bar{H}_i(x) - \delta_i m_i - k_i c_i, && \dot{\bar{p}}_i = \tilde{D} h_{i,3}(I_{i,3}) - \tilde{\delta}_i p_i - \beta_i c_{p_i}, \end{aligned} \tag{Equation S8}$$

in which we have used the relations $\beta_i \ll k_i$ and $m_i/K_M \ll 1$ as before. For this system, we seek to determine how large $\bar{D}$ must be to guarantee that $\dot{c}_i = \bar{s}_i (m_i/K_m)/(1 + p_i/K_d)$ in the $\dot{\bar{m}}_i$ equation becomes sufficiently small in a short time such that it becomes negligible. Specifically, we request that by the time $T(\varepsilon)$ at which $m_i(t)$ has decreased by ϵ x 100% with respect to m_i^*, the term $-k_i c_i$ has become negligible compared to $-\delta_i m_i$. If this is the case and ε is sufficiently small, at time T the state of the system $0.4 \cdot 10^{-3}$ will still be in the region of attraction of S_0 and since $\bar{s}_i (m_i/K_m)/(1 + p_i/K_d)$ can be neglected, the m_i dynamics (and hence those of the full system) are approximately the same as those of the original system without feedback controller. Since S_0 is stable for this system and the state at time T is in its region of attraction, the state will ultimately converge to S_0.

First, we find a lower bound for $T(\varepsilon)$ from analyzing the dynamics of m_i. To this end, since $\dot{\bar{m}}_i = \dot{m}_i + \dot{c}_i$, $\partial c_i / \partial p_i \leq 0$, $\partial c_i / \partial \bar{s}_i \geq 0$, and $\dot{p}_i \geq 0$, we have that $\dot{m}_i (1 + \partial c_i / \partial m_i) \geq \dot{\bar{m}}_i$. Since $\partial c_i / \partial m_i \leq \bar{s}_i / K_m$ and $\dot{\bar{m}}_i \geq -\delta_i m_i - k_i (\bar{s}_i / K_m) m_i$, we finally have that

$$\dot{m}_i \geq -G_i m_i, \quad m_i(0) = m_i^*,$$

in which we have used $\delta_i \ll G_i$. From this, it follows that $m_i(t) \geq m_i(0) e^{-G_i t}$ and therefore that $m_i(t) \geq (1 - \varepsilon) m_i(0)$ as long as

$$t \leq \frac{1}{G_i} \ln\left(\frac{1}{1 - \varepsilon}\right) = T(\varepsilon).$$

Second, we determine for what values of the copy number $\bar{D}$, we can guarantee that $k_i c_i(t) \leq 0.1 \delta_i m_i$ for all $t \geq T$, so that the term $k_i c_i$ can be neglected with respect to $\delta_i m_i$ after this time. To this end, consider that $\bar{s}_i(t) = e^{-\beta_i t} \bar{s}_i(0)$ with $\bar{s}_i(0) = (D \alpha_i / \beta_i)$, so that

$$k_i c_i(t) = \frac{k_i}{K_m} e^{-\beta_i t} \frac{D \alpha_i}{\beta_i} \frac{m_i}{1 + p_i/K_d}, \quad G_i = \frac{k_i D \alpha_i}{K_m \beta_i}.$$

It is therefore sufficient to request that

$$G_i e^{-\beta_i t} \frac{1}{1 + p_i(t)/K_d} \leq 0.1 \delta_i, \forall t \geq T. \tag{Equation S9}$$

To determine when this is the case, we analyze the $\dot{p}_i$ dynamics and determine the smallest value that $p_i(t)$ takes for $t \geq T$. From $\dot{\bar{p}}_i = \dot{p}_i + \dot{c}_{p_i}$, with $\partial c_{p_i} / \partial p_i = (\bar{s}_i / K_m)(1/(1 + p_1/K_d)^2)$, and using the expressions for $\dot{\bar{s}}_i$ and $\dot{\bar{p}}_i$ in Equation 11, we finally obtain

$$\dot{p}_i = \left(\tilde{D} h_{i,3}(I_{i,3}) - \tilde{\delta}_i p_i\right) \left(\frac{1}{1 + (\bar{s}_i/K_m) \Big/ (1 + p_i/K_d)^2}\right).$$

From this, employing differential inequalities, we obtain that

$$p_i(t) \geq \frac{\bar{D} h_{i,3}(I_{i,3})}{\tilde{\delta}_i} \left(1 - e^{-\lambda t}\right), \lambda = \frac{\tilde{\delta}_i}{1 + (\bar{s}_i(0)/K_m)}.$$

For ε sufficiently small, we can use Taylor expansion of $T(\varepsilon)$ to obtain that $T \approx \varepsilon/(G_i(1-\varepsilon))$. Letting $h_{i,3}(I_{i,3}) = \alpha_i$ as performed for the siRNA expression rate, we therefore have that

$$p_i(t) \geq \frac{\overline{D}\alpha_i}{\delta_i}\left(\frac{\lambda\varepsilon}{G_i(1-\varepsilon)}\right), \forall t \geq 0.$$

Substituting this expression into the left-hand side of Equation 11, we finally obtain

$$\frac{\overline{D}\alpha_i}{K_d}\varepsilon \geq 10\frac{G_i^2}{\delta_i}\left(1+\frac{\overline{s}_i(0)}{K_m}\right).$$

Here, we consider $K_d \approx 0.004$ nM, which corresponds to one among the smallest values given by thermodynamic estimates (Jens and Rajewsky, 2015). Using $\epsilon = 0.1$, $G_i = 10\delta_i$ ($D = 0.0002$ nM) as before, $\overline{s}_i(0) = D\alpha_i/\beta_i$, $\delta_i = \delta_2 = 0.09$ hr^{-1}, it is sufficient to have $\overline{D} \approx 0.54$ nM, corresponding to a DNA copy number of about 230. This number can be easily increased by increasing the number of sequences per DNA copy transcribed (Jens and Rajewsky, 2015).

Outer Loop Feedback Control for Adjusting x_i*

The inducers' concentrations uniquely determine the prescribed concentrations x_i* according to Equation 6. Setting the inducers' concentrations to $I_{i,1}$* may be difficult in practice because the parameters involved in Equation 6, even if they pertain to the synthetic genetic controller circuit, may not be exactly known. To overcome this problem, we consider a steady state feedback adjustment of the inducer level (Figure S3A). Specifically, the inducer levels are initialized based on a reasonable guess and then are iteratively adjusted based on the proximity of the resulting reached steady state x_i * to the target concentration x_i^{S0}. Since the measurement of x_i occurs only after this has reached its steady state x_i *, the measurement does not need to occur in real-time. In fact, the controller's effort "freezes" the network TFs' concentrations x_i at x_i * until the controller circuit's inducer levels are updated, thus allowing sufficient time for measurements to take place. Letting T be the time it takes for $x_i(t)$ to reach the proximity of x_i * and letting k denote a natural number, we can set the inducer level at time $t = (k+1)T$ based on its value at time kT and on the discrepancy between x_i^{S0} and x_i *. This leads to the feedback law

$$I_{i,1}((k+1)T) = I_{i,1}(kT) + K_i\left(x_i^{S_0} - x_i(kT)\right), \quad k \in \mathbf{N}, \qquad \text{(Equation 11)}$$

in which $x_i(kT) \approx x_i^*$ with $x_i^* = (\kappa_i/\gamma_i)(\beta_i h_{i,1}(I_{i,1}(kT))/\overline{k}_i\alpha_i)$. The comparison $x_i^{S_0} - x_i(kT)$ can be performed in a computer and the inducers can be adjusted via in silico computation as proposed by other works (Milias-Argeitis et al., 2011). In contrast to these previous studies, however, the inducer adjustment does not take place in real-time and instead takes place only after the concentration $x_i(t)$ has reached the proximity of its steady state value x_i^*, allowing for time consuming concentration quantifications to take place. A strategy where the network is directly controlled by an in silico controller would not necessarily guarantee stabilization of the TF's concentrations x_i to their prescribed values x_i^* due to delay-induced instabilities, as documented by other works (Menolascina et al., 2014). The presence of the stabilizing action of the high-gain synthetic genetic controller circuit overcomes this problem. Figure S3B reports simulation results with the two-node endogenous gene regulatory network of Figure 3A for different values of the coefficients K_1, K_2, showing that the system reaches a proximity of the target concentrations x^{S_0}. The choice of K_1 and K_2 affects the speed of convergence to the target state. Specifically, larger values lead to faster convergence but also to larger overshoot and may, when too large, compromise the stability of the inducer update law in Equation 11. More sophisticated inducer update laws may consider adaptive ways of setting the constants K_i through, for example, the use of gradient descent algorithms with numerical estimation of the gradient (Nocedal and Wright, 2000) or techniques such as extremum seeking control (Ariyur and Krstic, 2003).

Discovering Paths to Pluripotency

Here, we illustrate how the ability to accurately set and hold any TF's concentration to a prescribed value, which we can do with our controller circuit, can be employed as a way to discover paths to reprogramming. To this end, we consider the case in which we control only a subset of the TFs of the pluripotency gene regulatory network. If this subset alone is sufficient to dictate the pluripotent state, then setting the concentrations of the TFs in this set to their pluripotent values will reprogram the network to pluripotency. If the TFs alone are not sufficient to dictate the pluripotent state, we can still leverage the ability to accurately set and hold their concentrations at prescribed values as illustrated in the following simple example.

Assume that the gene regulatory network that we want to reprogram has two TFs and that we can overexpress only one of them. The same reasoning follows if the network has many more TFs and we can overexpress a subset of them, but the graphical illustrations become cumbersome. Let the two TFs be denoted by x_1 and x_2 in which we are allowed to overexpress only x_2. As a concrete example, we can think of x_1 as being Nanog and x_2 as being Oct4, and model an experiment in which we seek to reprogram the network to PL by accurate control of Oct4 only. The network model is given by

$$\sum_u : \dot{x}_1 = \frac{a_1x_1^2 + b_1x_2^2 + c_1x_1^2x_2^2}{1 + x_1^2 + x_2^2 + x_1^2x_2^2 + ex_2^4} - \gamma_1x_1, \quad \dot{x}_2 = \frac{a_2x_1^2 + b_2x_2^2 + c_2x_1^2x_2^2}{1 + x_1^2 + x_2^2 + x_1^2x_2^2} - \gamma_2x_2 + u_2 \qquad \text{(Equation S10)}$$

For a representative parameter choice leading to three stable steady states (PL, PE, and TR), the nullclines and vector field for $u_2 = 0$ are given in Figure S3C, in which we have highlighted in red the target pluripotent state (PL). If we apply $u_2 = G_2(x_2^* - x_2)$ with G_2 sufficiently large while $u_1 = 0$, the controller guarantees that $x_2(t)$ is steered toward x_2^* while the steady state value that $x_1(t)$ reaches depends on the shape of the $\dot{x}_1 = 0$ nullcline (Figure S3D). If the concentration of x_2 alone were sufficient to determine the PL state, then, referring to Figure S3D, the horizontal line with $x_2^* = 2$ passing through PL would have only one stable intersection with the black nullcline. In the plot shown, instead, it has two stable intersections, one at PL and one at a point denoted by x^1 closer to the initial condition $x(0)$. Thus, setting $x_2^* = a$ will result into a trajectory that approaches x^1 (light blue) instead of PL. However, if we keep increasing the prescribed value x_2^* in small steps, we will eventually drive the state of the system to x^2 and then to x^3. At this point, we can set the prescribed value back to $x_2^* = a$ and the state will converge to PL. This is an example in which progressively setting x_2^* to a, then to b, then to c, and then back to a gives a different outcome for the system's state x from setting x_2^* directly to a. In this case, the chosen sequence of steady state concentrations for the TF that we can control determines the end state of the network. This example also shows that progressive increase and then decrease of the prescribed concentrations x_i^* of the TFs that we can control may be a promising approach to find a path to reprogramming if one exists.

High Gain and Noise in the Genetic Controller

Considering the simple ODE model of the total species concentrations m_i and x_i with the synthetic genetic controller in Equation 7, which for G_i sufficiently large becomes

$$\frac{dm_i}{dt} = G_i\left(m_i^* - m_i\right), \quad \frac{dx_i}{dt} = \kappa_i m_i - \gamma_i m_i.$$

Here, we seek to mathematically demonstrate on this simple model that increased gain G_i in the feedback controller decreases the coefficient of variation of x_i. To this end, we consider the corresponding Chemical Langevin Equation (CLE) to the above system given by

$$\frac{dm_i}{dt} = G_i\left(m_i^* - m_i\right) + \sqrt{G_i m_i^* + G_i m_i m}\,\Gamma_m, \quad \frac{dm_i}{dt} = \kappa_i m_i - \gamma_i x_i + \sqrt{\kappa_i m_i - \gamma_i x_i}\,\Gamma_x,$$

in which Γ_m and γ_x are realizations of white noise processes. Since the system has linear propensities, the moments equations are closed and therefore we will use them to obtain the variance and the mean of x_i. These equations are given by

$$\frac{d\mathbb{E}[m_i]}{dt} = G_i\left(m_i^* - \mathbb{E}[m_i]\right), \quad \frac{d\mathbb{E}[x_i]}{dt} = \kappa_i\mathbb{E}[m_i] - \gamma_i\mathbb{E}[x_i]$$

$$\frac{d\mathbb{E}\left[m_i^2\right]}{dt} = G_i\mathbb{E}[m_i]\left(1 + 2m_i^*\right) + G_i m_i^* - 2G_i\mathbb{E}\left[m^2\right],$$

$$\frac{d\mathbb{E}\left[x_i^2\right]}{dt} = 2\kappa_i\mathbb{E}[m_i x_i] - 2\gamma_i\mathbb{E}\left[x_i^2\right] + \kappa_i\mathbb{E}[m_i] + \gamma_i\mathbb{E}[x_i],$$

$$\frac{\mathbb{E}[m_i x_i]}{dt} = G_i m_i^*\mathbb{E}[x_i] - \mathbb{E}[m_i x_i](\gamma_i + G_i) + \kappa_i E\left[m_i^2\right].$$

Setting these to the steady state, and calculating the steady state variance of m_i and x_i, we obtain

$$\mathrm{Var}(m_i) = m_i^*, \quad \mathrm{Var}(x_i) = \frac{m_i^*\kappa_i}{\gamma_i}\left(1 + \frac{\kappa_i}{G_i + \gamma_i}\right)$$

leading to the following coefficients of variation:

$$CV_m > \frac{\sqrt{\mathrm{Var}(m_i)}}{\mathbb{E}[m_i]} = \frac{1}{\sqrt{m_i^*}} \quad CV_x > \frac{\sqrt{\mathrm{Var}(x_i)}}{\mathbb{E}[x_i]} = \frac{\sqrt{\left(1 + \frac{\kappa_i}{G_i + \gamma_i}\right)}}{\sqrt{\frac{m_i^*\kappa_i}{\gamma_i}}}$$

From the expression of CV_x, we conclude that as G_i is increased the coefficient of variation of x_i decreases. Furthermore, since the gain G_i does not affect the mean value of x_i, increased G_i will simply reduce the variance of x_i.

Stochastic Model

Stochastic differential equation (SDE) models for the endogenous pluripotency circuit of Oct4 and Nanog as well as the controller and its shutdown via sponge mRNAs were constructed from the reactions surrounding Nanog and Oct4 promoter regulation. Reaction channels for processes such as mRNA translation, siRNA-mRNA interaction and species dilution and degradation were explicitly accounted for as well (Table S2). Noise in all these processes was captured by employing the Chemical Langevin Equation (CLE) for describing the dynamic behavior of molecular species and their associated reaction channels taking place in a well-stirred reaction volume Ω (Gillespie, 2000). Each reaction channel j was assigned a propensity function a_j to govern the rate of its procession; for unimolecular reactions of the form $X \xrightarrow{k} Y$, the propensity function is a function of the number of molecules of X: $a_j = k \cdot X$ while for bimolecular reactions of the form $X + Y \xrightarrow{k} Z$, the propensity function is $a_j = (k/\Omega) \cdot XY$ (Del Vecchio and Murray, 2014),

Endogenous Network

The endogenous network of Figure B1A was modeled with the following 15 *dynamic variables*: transcription factor dimers N_2 (representing Nanog-Nanog) (Wang et al., 2008; Mullin et al., 2008) and O_2 (representing Oct4-Sox2) (Tapia et al., 2015), transcription factors N and O (Nanog and Oct4, respectively), their mRNA precursors m_N and m_O free Nanog and Oct4 DNA promoters D_N and D_O, single-bound promoters D_{NO}, D_{ON}, D_{NN}, D_{OO} (where D_{ij} represents the dimer of species *j* bound to promoter of species *i*), double-bound promoters D_{NNO}, D_{ONO} (where D_{ijk} represents the dimer of species *k* bound to the single-bound promoter D_{ij}), and D_X, the transcriptionally inactive form of Nanog promoter being repressed by an Oct4 dimer. The reaction channels pertaining to these variables are listed in Table S2A.

Controller

The downregulatory function of the controller is modeled by the inducible transcription (through inducer $I_{i,2}$, whose activation is modeled with the Hill function $h(I_{i,2})$ as in Results section entitled: ''Implementation of feedback overexpression of TF x_i through a synthetic genetic controller circuit'') of siRNA strands for the species s_N and s_O from DNA with copy number D_{cn} and D_{co}, respectively. The siRNA species s_N and s_O bind to and degrade the mRNA species m_N and m_O respectively, forming the intermediate complexes c_N and c_O along their degradation pathways. Additionally, the upregulatory function of the controller is modeled with the inducible transcription (through inducer $I_{i,1}$ activating with the Hill function $h(I_{i,1})$) of the TF genes for Nanog and Oct4 on DNA with copy numbers D_{cn} and D_{co}. The reaction channels pertaining to these controller variables are listed in Table S2B.

Sponge mRNA for Controller Shutdown

Shutdown of the controller is modeled with inducible transcription (through inducer $I_{i,3}$ whose activation is modeled with the Hill function $h(I_{i,3})$ as in the STAR Methods subsection entitled ''Feedback Controller Shutdown'' above) of sponge mRNA species p_N and p_O, which bind to and sequester the siRNA species s_N and s_O, respectively. Along this sequestration pathway, the intermediate complexes $c_{p,N}$ and $c_{p,O}$ are formed. The reaction channels pertaining to these sponge mRNA species are listed in Table S2C.

Overexpression in the endogenous circuit is represented by a birth process for O and N at time-constant rates u_N and u_O. These are represented through the reaction channels in Table S2D.

Chemical Langevin Equations

From the reaction channels listed in Table S2 for the 23 species of the collective endogenous, controller, and sponge mRNA molecules described above, the CLE listed in full in Data S1 (Document S1) was constructed.

In these SDEs, the terms Γ_j represent the white noise associated with reaction channel *j*. The endogenous circuit (Figure B1A) is realized by setting the inducers on the controller and sponge to $h(I_{i,1}) = h(I_{i,2}) = h(I_{i,3}) = 0$ for $i \in \{N, O\}$. Realizations of the controller circuit (Figure B1D) that steers the system's state to the arbitrary unit values of (N^*, O^*) = (184,25) were obtained by setting the inducers $h(I_{i,1}) \equiv h_{i,1}$ and $h(I_{i,2}) \equiv h_{i,2}$ for $i \in \{N, O\}$ in the model above to the nonzero levels listed in Table S3. Note that $h(I_{i,1})$ is set as a function of this target state as obtained from the results of the STAR Methods subsection entitled ''Synthetic Genetic Feedback Controller Circuit'': $h(I_{i,1}) = (X_i^* \cdot \gamma_i \cdot h(I_{i,2}) \cdot k_{si})/(\kappa_i \cdot K_{mi} \cdot \beta_i)$. By the same token, $h(I_{i,2})$ is arbitrarily set in accordance with the design of the controller as first an siRNA saturating device followed by the right level of synthetic mRNA upregulation to achieve the target state. Shutdown of the controller with the sponge mRNA was realized by again setting $h(I_{i,1}) = h(I_{i,2}) = 0$ while also setting $h(I_{i,3}) \equiv h_{i,3}$ to the values in Table S3.

The Euler-Marayuma Method (Kloeden and Platen, 1992) was implemented using MATLAB R2015b to obtain approximate numerical solutions to the respective system of SDEs in the realization of these circuits. The parameters used are listed in Tables S1 and S3, with $\Omega = 10^{1.9}$. The Γ_j terms for each channel were computed using a discretized Wiener process for timestep $dt : \Gamma_j = N(0, 1/dt) = \sqrt{dt} \cdot N(0, 1)$, where $N(0, 1)$ is the normal distribution and is sampled in MATLAB using the pseudorandom generator function *randn*.

Fixed Overexpression and Stochastic Transitions

It is possible to re-design the deterministic landscape of Figure B1B such that there is a chance that fixed overexpression leads to reprogramming from the TR state to the PL state. With parameters as given in Figure S4, the deterministic landscape allows for choices of u_1 and u_2 that cause the TR state to disappear before the PL state, thus enabling a TR to PL state transition. Figure S4 shows realizations of the Chemical Langevin Equation model in Data S1 (Document S2), derived from the endogenous reactions detailed in Table S2A, and parameters as shown. From the figure, it appears that while successful transitions from TR to PL is possible via fixed overexpression, the weak stability of the PL state under overexpression causes noise to eventually push the state out of the PL basin of attraction. This is in contrast to the controller, which enforces the prescribed concentrations as long as it is kept on.

Published Models of the Pluripotent Network

In Faucon et al. (2014), a computational high-throughput screening of fully connected, three node network architectures (Fully Connected Triads; FCTs) indicated that mutually activating FCTs in which the nodes also self-activate are among the architectures with the highest probability of multistability. The screenings were performed using ODE models that captured activation and repression additively, in contrast to the model considered in this paper, which captures transcriptional regulation using cooperative Hill functions to account for the known co-binding of these factors on the promoters they regulate (Boyer et al., 2005). In Chickarmane et al. (2006), the fully connected triad (FCT) of Oct4, Sox2, and Nanog was modeled in a four dimensional ODE model that tracked the evolution of concentrations of Oct4, Sox2, Nanog, and the heterodimer Oct4-Sox2 ([O],[S],[N],[OS], respectively). In contrast, the model in this paper lumped together Oct4 and Sox2 into a single variable (O^2), and treated the OS heterodimer as this complex. Furthermore, our model treated Nanog as a homodimer when transcriptionally regulating promoters (Wang et al., 2008; Mullin et al., 2008). In

Kalmar et al. (2009), a two dimensional auto and mutually activating motif between Oct4 and Nanog also included repressive regulation from Oct4 onto Nanog at sufficiently high concentrations of Oct4. However, this model treated Nanog as a monomer and used an entirely different species that represented Oct4 at higher concentrations. In Shu et al. (2013), an ODE model of four variables was used, which included Oct4, Sox2, ME, and ECT. The latter two variables represent the family of mesendodermal (ME) and ectodermal (ECT) genes, respectively. In contrast, this paper used a model that was limited to the core pluripotency network of master regulators (Oct4, Sox2, and Nanog). In Chickarmane and Peterson (2008), a computational model capturing the same three phenotypes in this paper (pluripotent, trophectoderm, and primitive endoderm) was used. In addition to treating Oct4, Sox2, and Nanog as nodes in the network, this model included variables modeling the lineage specifiers Cdx2 and Gata6 as well as GCNF, while also treating Nanog as a monomer and the heterodimer Oct4-Sox2 as its own variable. In Li and Wang (2013), a 52-node ODE model of the stem cell network was analyzed in the context of two basins of attraction representing the stem cell progenitor state and the differentiated state. The ODEs in this model captured activation and repression using additive Hill functions.

In Faucon et al. (2014), a computational high-throughput screening of fully connected, three node network architectures (Fully Connected Triads; FCTs) indicated that mutually activating FCTs in which the nodes also self-activate are among the architectures with the highest probability of multistability. The screenings were performed using ODE models that captured activation and repression additively, in contrast to the model considered in this paper, which captures transcriptional regulation using cooperative Hill functions to account for the known co-binding of these factors on the promoters they regulate (Boyer et al., 2005). In Chickarmane et al. (2006), the fully connected triad (FCT) of Oct4, Sox2, and Nanog was modeled in a four dimensional ODE model that tracked the evolution of concentrations of Oct4, Sox2, Nanog, and the heterodimer Oct4-Sox2 ([O],[S],[N],[OS], respectively). In contrast, the model in this paper lumped together Oct4 and Sox2 into a single variable (O^2), and treated the OS heterodimer as this complex. Furthermore, our model treated Nanog as a homodimer when transcriptionally regulating promoters (Wang et al., 2008; Mullin et al., 2008). In Kalmar et al. (2009), a two dimensional auto and mutually activating motif between Oct4 and Nanog also included repressive regulation from Oct4 onto Nanog at sufficiently high concentrations of Oct4. However, this model treated Nanog as a monomer and used an entirely different species that represented Oct4 at higher concentrations. In Shu et al. (2013), an ODE model of four variables was used, which included Oct4, Sox2, ME, and ECT. The latter two variables represent the family of mesendodermal (ME) and ectodermal (ECT) genes, respectively. In contrast, this paper used a model that was limited to the core pluripotency network of master regulators (Oct4, Sox2, and Nanog). In Chickarmane and Peterson (2008), a computational model capturing the same three phenotypes in this paper (pluripotent, trophectoderm, and primitive endoderm) was used. In addition to treating Oct4, Sox2, and Nanog as nodes in the network, this model included variables modeling the lineage specifiers Cdx2 and Gata6 as well as GCNF, while also treating Nanog as a monomer and the heterodimer Oct4-Sox2 as its own variable. In Li and Wang (2013), a 52-node ODE model of the stem cell network was analyzed in the context of two basins of attraction representing the stem cell progenitor state and the differentiated state. The ODEs in this model captured activation and repression using additive Hill functions.